

8-7-2023

## A Biologic-Device Combination Product Delivering Tumor-Derived Antigen Elicits Immunogenic Cell Death-Associated Immune Responses Against Glioblastoma

Christopher Cultrara

Christopher Uhl

Kenneth Kirby

Essam Abed Elrazaq

Amelia Zellander

*See next page for additional authors*

Follow this and additional works at: <https://jdc.jefferson.edu/neurosurgeryfp>



Part of the [Neurology Commons](#), [Oncology Commons](#), and the [Surgery Commons](#)

**[Let us know how access to this document benefits you](#)**

---


This Article is brought to you for free and open access by the Jefferson Digital Commons. The Jefferson Digital Commons is a service of Thomas Jefferson University's [Center for Teaching and Learning \(CTL\)](#). The Commons is a showcase for Jefferson books and journals, peer-reviewed scholarly publications, unique historical collections from the University archives, and teaching tools. The Jefferson Digital Commons allows researchers and interested readers anywhere in the world to learn about and keep up to date with Jefferson scholarship. This article has been accepted for inclusion in Department of Neurosurgery Faculty Papers by an authorized administrator of the Jefferson Digital Commons. For more information, please contact: [JeffersonDigitalCommons@jefferson.edu](mailto:JeffersonDigitalCommons@jefferson.edu).

---

**Authors**

Christopher Cultrara, Christopher Uhl, Kenneth Kirby, Essam Abed Elrazaq, Amelia Zellander, David W. Andrews, Charles B. Scott, Lorenzo Galluzzi, Mark A. Exley, and Jenny Zilberberg

# A biologic-device combination product delivering tumor-derived antigens elicits immunogenic cell death-associated immune responses against glioblastoma

Christopher Cultrara,<sup>1</sup> Christopher Uhl,<sup>1</sup> Kenneth Kirby,<sup>1</sup> Essam Abed Elrazaq,<sup>1</sup> Amelia Zellander,<sup>1</sup> David W Andrews,<sup>2,3</sup> Charles B Scott,<sup>4</sup> Lorenzo Galluzzi,<sup>5,6,7</sup> Mark A Exley,<sup>1</sup> Jenny Zilberberg <sup>1</sup>

**To cite:** Cultrara C, Uhl C, Kirby K, *et al.* A biologic-device combination product delivering tumor-derived antigens elicits immunogenic cell death-associated immune responses against glioblastoma. *Journal for ImmunoTherapy of Cancer* 2023;**11**:e006880. doi:10.1136/jitc-2023-006880

► Additional supplemental material is published online only. To view, please visit the journal online (<http://dx.doi.org/10.1136/jitc-2023-006880>).

CU and KK contributed equally.  
Accepted 21 July 2023



© Author(s) (or their employer(s)) 2023. Re-use permitted under CC BY-NC. No commercial re-use. See rights and permissions. Published by BMJ.

For numbered affiliations see end of article.

**Correspondence to**  
Dr Jenny Zilberberg;  
[jenny@discordia.org](mailto:jenny@discordia.org)

## ABSTRACT

**Background** IGV-001 is a personalized, autologous cancer cell-based immunotherapy conceived to deliver a tumor-derived antigenic payload in the context of immunostimulatory signals to patients with glioblastoma (GBM). IGV-001 consists of patient-derived GBM cells treated with an antisense oligodeoxynucleotide against insulin-like growth factor 1 receptor (IGF1R) and placed in proprietary biodiffusion chambers (BDCs). The BDCs are then exposed to 5–6 Gy radiation and implanted at abdominal sites for ~48 hours. IGV-001 has previously been shown to be generally safe with promising clinical activity in newly diagnosed GBM patients.

**Methods** Mouse (*m*) or human (*h*) variants of IGV-001 were prepared using GL261 mouse GBM cells or human GBM cells, respectively. BDCs containing vehicle or *m*IGV-001 were implanted in the flanks of C57BL/6 albino female mice in preventative and therapeutic experiments, optionally in combination with a programmed cell death 1 (PD-1) blocker. Bioactivity of the general approach was also measured against hepatocellular carcinoma Hepa 1–6 cells. Mice were followed for the growth of subsequently implanted or pre-existing tumors and survival. Draining lymph nodes from mice receiving *m*IGV-001 were immunophenotyped. *m*IGV-001 and *h*IGV-001 were analyzed for extracellular ATP and high mobility group box 1 (HMGB1) as indicators of immunogenic cell death (ICD), along with flow cytometric analysis of viability, surface calreticulin, and reactive oxygen species. Stress and cell death-related pathways were analyzed by immunoblotting.

**Results** IGV-001 causes oxidative and endoplasmic reticulum stress in GL261 cells, resulting in a cytotoxic response that enables the release of antigenic material and immunostimulatory, ICD-associated molecules including ATP and HMGB1 from BDCs. Immunophenotyping confirmed that IGV-001 increases the percentage of dendritic cells, as well as effector, and effector memory T cells in BDC-draining lymph nodes. Consistent with these observations, preventative IGV-001 limited tumor progression and extended overall survival in mice intracranially challenged with GL261 cells, a benefit that was associated with an increase in tumor-specific

## WHAT IS ALREADY KNOWN ON THIS TOPIC

⇒ IGV-001, a biologic-device combination product, has been shown to be safe and mediate potential efficacy in a Phase I clinical trial enrolling patients with glioblastoma (GBM).

## WHAT THIS STUDY ADDS

⇒ We demonstrate that IGV-001 can induce oxidative and endoplasmic reticulum stress on GBM cells in the product, resulting in immunogenic cell death and consequent antitumor immunity.

## HOW THIS STUDY MIGHT AFFECT RESEARCH, PRACTICE OR POLICY

⇒ This study supports the use of IGV-001 as a therapeutic modality in GBM, while providing data on its mechanism of action.

T cells with effector features. Similar findings were obtained in the Hepa 1–6 model. Moreover, therapeutically administered IGV-001 combined with PD-1 delayed progression in GBM-bearing mice.

**Conclusions** These results support treatment with IGV-001 to induce clinically relevant ICD-driven anticancer immune responses in patients with GBM.

## INTRODUCTION

Glioblastoma (GBM) is the most prevalent and lethal primary brain malignancy in adults.<sup>1</sup> Standard of care (SOC) for GBM generally consists in maximal safe surgical resection followed by adjuvant radiation therapy (RT) plus temozolomide, followed by temozolomide-based maintenance.<sup>2</sup> GBM is well known for its elevated spatial and temporal intertumoral and intratumoral heterogeneity,<sup>3 4</sup> pointing to a suboptimal clonal control by cytotoxic T lymphocytes (CTLs) and hence phenotypic clonal

divergence.<sup>5</sup> Consistent with this observation, the GBM tumor microenvironment (TME) is generally enriched with immunosuppressive cells that hinder CTL functionality,<sup>4,6,7</sup> contributing to a pronounced resistance to immune checkpoint inhibitors (ICIs) and other immunotherapeutic agents. Indeed, nivolumab, an ICI targeting programmed cell death 1 (PDCD1, best known as PD-1), failed to improve outcomes as compared with vascular endothelial growth factor A (VEGFA) neutralization with bevacizumab, which is approved for the treatment of GBM,<sup>8</sup> in patients with recurrent GBM.<sup>9</sup> Chimeric antigen receptor (CAR)-expressing T cells targeting a GBM-associated variant of epidermal growth factor receptor (EGFR) also did not improve the survival of patients with GBM.<sup>10</sup> Similarly, various therapeutic cancer vaccines that have been or are being clinically evaluated in patients with GBM have yet to provide compelling therapeutic benefits to this patient population.<sup>11–15</sup>

IGV-001 is an autologous cancer cell-based immunotherapeutic approach conceived to deliver an antigenic payload in the context of immunostimulatory molecules to patients with GBM. Specifically, IGV-001 consists of autologous GBM cells that are (1) incubated with an antisense oligodeoxynucleotide (IMV-001) targeting insulin-like growth factor 1 receptor (IGF1R), (2) placed in proprietary biodiffusion chambers (BDCs) of 0.1 μm pore size together with additional IMV-001, (3) exposed to radiation in a single dose of 5–6 Gy, and (4) implanted in patients at abdominal sites (ie, at distance from the immunosuppressive GBM TME and draining lymph nodes).<sup>16</sup> IGV-001 is advantageous in that it comprises an unselected population of cancer cells, thereby including a broad antigenic signature of each tumor. Moreover, the BDC pore size allows for the selective release of relatively small subcellular tumor particles, which are taken up efficiently by immunostimulatory dendritic cells (DCs)<sup>17,18</sup> while preventing contact between dying cancer cells and macrophages, which generally promote immunosuppression.<sup>19,20</sup> IGV-001 has recently been evaluated in patients with newly diagnosed GBM as part of a Phase 1b clinical trial (NCT02507583). Specifically, IGV-001 was manufactured shortly after tumor resection (during patient hospitalization) and administered 4–6 weeks prior to SOC adjuvant RT plus temozolomide-based chemotherapy. In this context, median overall survival (OS) of ‘Stupp-eligible’ patients (n=10) receiving the highest IGV-001 exposure was 38.2 months as compared with 16.2 months in recent patients receiving SOC therapy (p=0.044).<sup>16</sup> Importantly, these findings led to the initiation of a follow-up Phase 2b study (NCT04485949) and prompted preclinical exploration to unravel the mechanism of action of IGV-001.

Importantly, cancer cells can respond to stress (including mechanical and RT-elicited stress) in a variety of ways, ranging from the activation of survival pathways that support the restoration of cellular homeostasis to the initiation of molecular cascades precipitating regulated cell death (RCD).<sup>21</sup> While RCD is obviously

desirable in the context of cancer therapy, multiple signal transduction pathways that often accompany RCD actively suppress the initiation of cancer-specific immune responses, potentially limiting the overall efficacy of treatment.<sup>22</sup> Conversely, specific therapeutic approaches including various chemotherapies<sup>23</sup> and targeted anti-cancer agents,<sup>24</sup> RT (at least when used according to precise dose and fractionation schedules),<sup>25</sup> as well as photodynamic therapy<sup>26</sup> can all elicit an immunologically proficient variant of RCD commonly known as ‘immunogenic cell death’ (ICD), which culminates with the activation of tumor-targeting immunity in support of treatment efficacy.<sup>22</sup>

Using both murine and human GBM cell lines as well as patient-derived GBM cells, here we demonstrate that IGV-001 rapidly (<48 hours) elicits several ICD-associated immunostimulatory signals in support of tumor-targeting immunity.

## MATERIALS AND METHODS

### Cell lines

Luciferase-expressing GL261 mouse GBM cells (GL261-luc2) were obtained from PerkinElmer (by Labcorp). The GL261 cell line was purchased from DSMZ (Leibniz Institute, DE; ACC 802). JAWS II (CRL-11904) mouse immature DC, T98G (CRL-1690) and U-87 MG (HTB-14; herein referred to as U87) human GBM cell lines were purchased from the American Type Culture Collection (ATCC). Culture media was prepared according to provider’s recommendations with Roswell Park Memorial Institute (RPMI)-1640 or Eagle’s Minimum Essential Medium and supplemented with 10% fetal bovine serum (FBS) and 1% penicillin/streptomycin. Cultures were maintained at 37°C under 5% CO<sub>2</sub> according to the provider’s instructions.

### Primary GBM cell isolation

Clinical samples were obtained with patient consent under Thomas Jefferson University’s Clinical Study Protocol #TJU-14379–102, Version #102.0. GBM tumors were collected under Jefferson’s approved tissue procurement protocol Control #21C.030 and shipped in normal saline in temperature-controlled (2–8°C) containers. Resected tumor material was minced and dissociated at 37°C using a proprietary enzyme cocktail. After dissociation, the cell pellet was red blood cell (RBC) lysed, passed through a 40 μm cell strainer, resuspended in saline, and counted. Culture medium for experiments involving patient-derived GBM cells used Human Plasma-Like Media (Thermo Fisher Scientific, California, USA) supplemented with 5% human serum and 1% penicillin/streptomycin.

### IGV-001 formulation and culture

For the preparation of *m*IGV-001 (GL261-luc2 or GL261) and *h*IGV-001 (T98G or U87), cell lines were grown to ~80% confluency in T75 tissue culture flasks and then

treated with IMV-001 (Nitto Denko AVECIA, Massachusetts, USA) for 3 hours. After treatment, cells were harvested, washed with complete media, resuspended in 0.9% saline (SteriCare Solutions, Texas, USA) with additional IMV-001 and counted. The cell suspension (365  $\mu$ L) was loaded into pre-made BDCs [0.1  $\mu$ m-pore size, polyvinylidene difluoride (PVDF) membrane] at a density of  $5 \times 10^5$ – $1 \times 10^6$  cells/BDC and then irradiated with 5–6 Gy (225 kV) X-rays using a MultiRad irradiator (Precision X-Ray Irradiation, CT). IGV-001 was prepared with patient-derived tumor cells as previously described, with modifications.<sup>16</sup> For in vitro experiments, BDCs were placed into 12-well tissue culture plates containing 750  $\mu$ L of complete media, covered with 200  $\mu$ L more media and incubated at 37°C under 5% CO<sub>2</sub> atmosphere for 24–48 hours. Due to passive diffusion, 200  $\mu$ L of media was added to the top of each BDC every 24 hours to maintain moisture across both membranes and supply the cells with a minimal flow of nutrients. For cell death inhibition studies, GL261 cells pretreated for 3 hours with 25  $\mu$ M zVAD-fmk, 30  $\mu$ M necrostatin-1 (Nec-1), 1  $\mu$ M ferrostatin-1 (Fer-1), or 1–2 mM N-acetyl cysteine (NAC) (Sigma Aldrich, Missouri, USA). Following manufacturing, *m*IGV-001 was further co-incubated with inhibitors at the same concentrations for 24 hours.

#### Orthotopic GL261-luc2 mouse glioma model and lymph node immune response in vivo

In vivo murine studies were designed by Imvax, and executed by Labcorp in compliance with the National Institutes of Health and Labcorp's Animal Care and Use Committee or at Rutgers, the State University of New Jersey at an Association for Assessment and Accreditation of Laboratory Animal Care International (AAALAC)-accredited animal facility, under an Institutional Animal Care and Use Committee (IACUC)-approved protocol. Female C57BL/6 albino mice or male C57BL/6 mice received either BDCs filled with phosphate buffered saline (PBS) (control mice) or formulated *m*IGV-001 ( $1 \times 10^6$  GL261-luc2 cells/BDC, one BDC/mouse). BDCs were subcutaneously implanted in the flank for 48 hours followed by explantation and wound closing. On day 26 after BDC explantation, mice received an intracranial inoculation of  $1 \times 10^6$  GL261-luc2 cells to generate orthotopic tumors. T-cell subsets were depleted using anti-CD4 (clone GK1.5) or anti-CD8 antibody (clone 2.43) (Bio X Cell; 500  $\mu$ g/dose/animal on days 0–2, and 200  $\mu$ g/dose/animal on days 5, 8, 11, 14, 17, 20, 23, 26, all administered intraperitoneally). Tumor burden was evaluated using weekly bioluminescent imaging (BLI) of injected D-luciferin conversion with an IVIS Spectrum imager (Perkin-Elmer, Missouri, USA). Mice were euthanized before study termination when ethical abortion criteria were reached (eg, body weight loss  $\geq 20\%$ , signs of sickness, distended cranium, severely impaired movement, severe respiratory distress or loss of righting reflex). Lymph nodes (draining and contralateral) from mice that received *m*IGV-001 (GL261-luc2) were immunophenotyped by flow

cytometry. To enhance the response, 26 days after explantation, mice received a subcutaneous (SC) boost with  $1 \times 10^7$  GL261-luc2 cells/0.2 mL and lymph node collection was performed 7 days later. Additional methods for GL261 therapeutic setting and hepatocellular carcinoma models can be found in online supplemental methods and materials section.

#### Serum cytokine analysis

Blood serum samples were isolated at end of life and circulating levels of interferon gamma (IFN- $\gamma$ , best known as IFN- $\gamma$ ), interleukin-10 (IL-10), and interleukin-6 (IL-6) were measured by Luminex analysis using a MILLIPLEX MAP mouse CD8<sup>+</sup> T-cell premixed kit on a MAGPIX Luminex xMAP reader (Sigma Aldrich, Missouri, USA) as per the manufacturer's protocol. Serum samples were also taken to coincide with tumor burden BLI measurements. Circulating levels of IL-6 were also quantitated using a V-PLEX Proinflammatory Panel I (Meso Scale Discovery). Circulating levels of IL-6 evaluated on days 1, 14, and 28 days were correlated with BLI measurements on days 6, 13, and 27. At each time point and for each mouse receiving *m*IGV-001 (n=34), IL-6 levels were assigned to "Progressed" or "Stable" if the natural logarithm Ln(BLI total flux) > 20 or Ln(BLI total flux) < 20, respectively.

#### Tumor-specific T-cell assays

Peripheral blood mononuclear cells (PBMCs) collected on day 1 post-tumor challenge or splenocytes collected at end-of-life from control mice and surviving *m*IGV-001 treated mice were used in FluoroSpot or ELISpot assays to measure IFN- $\gamma$  production by T cells. PBMCs were stimulated using tumor lysate-pulsed DCs and splenocytes were incubated with major histocompatibility complex (MHC)-I H-2Db and H-2Kb GL261-specific peptides<sup>27</sup> (CHI Scientific). IFN- $\gamma$  was measured using a murine IFN- $\gamma$  capture FluoroSpot kit (CTL) or mouse IFN- $\gamma$  ELISpot Kit (R&D Systems). IFN- $\gamma$  counts were evaluated in an ImmunoSpot S6 UNIVERSAL Analyzer (CTL) or S6 Ultimate-V Analyzer (CTL).

#### ATP and high mobility group box 1 release

Supernatants from *m*IGV-001 and *h*IGV-001 BDCs were isolated at indicated time points, clarified by centrifugation, and stored at  $-80^\circ\text{C}$  for later analysis. Similarly, IGV-001 BDC contents from a Phase 1b clinical trial<sup>16</sup> were stored at  $-80^\circ\text{C}$  on BDC explantation. Extracellular high mobility group box 1 (HMGB1) was quantified by ELISA kit (Tecan, Switzerland) and extracellular ATP (eATP) was quantified using luciferase-luciferin RealTime-Glo eATP Assay (Promega, Wisconsin, USA), as per manufacturer's protocols. Measurements were recorded on a Cytation 5 Cell Imaging Multimode Reader (BioTek Instruments, Vermont, USA). Saline-loaded BDCs without cells were used as a vehicle control for both HMGB1 and eATP analyses. ATP release was also assessed after the IGV-001 manufacturing process.

Cell death and reactive oxygen species (ROS) quantification by flow cytometry *mIGV-001* and *hIGV-001* or patient-derived IGV-001 cells were retrieved from BDCs after 0, 24 or 48 hours and viability was assessed via annexin V and 7-AAD staining (BioLegend, California, USA), NucView 488 staining (Biotium, California, USA) for caspase 3–7 activity, and MitoView 633 for mitochondrial membrane potential, as per manufacturer's recommendations. Recovered cells were washed and resuspended in either binding buffer containing annexin V PeCy7 conjugate with 7-AAD or PBS plus 5% FBS containing NucView-488 or MitoView 633 substrates and incubated for 15 min at room temperature or 37°C in the dark. Stained cells were diluted in an appropriate buffer and then analyzed on a MACSQuaroon Analyzer 16 flow cytometer (Miltenyi Biotec, Germany). Cell counting via trypan blue exclusion was also used. Flow cytometric data analysis was performed using the Kaluza Analysis Software (Beckman Coulter, California, USA) package. *mIGV-001* and *hIGV-001* cells harvested from BDCs after 24 hours with or without NAC treatment were washed twice in PBS plus 5% FBS and ROS was determined via ROS Detection Assay Kit (Abcam, UK) using the 2',7'-dichlorodihydrofluorescein diacetate (H2DCFDA) oxidation system as per manufacturer's protocol. Data was collected on a MACSQuant Analyzer 16 flow cytometer and analysis was performed using the Kaluza Analysis Software package. An aliquot of stained cells was further counter-stained with 4', 6-diamidino-2-phenylindole (DAPI) and then imaged on an EVOS Cell Imaging system (Thermo Fisher Scientific, California, USA), maintaining consistent exposure time and light intensity for each time point.

Analysis of IGV-001 immediately after manufacturing was used as control to determine flow cytometry gating strategies for further time points.

### Immunoblotting

Cell pellets from *mIGV-001* were harvested at 0, 2, and 24 hours post preparation and lysed in a RIPA buffer containing 1× protease and phosphatase inhibitors (Thermo Fisher Scientific, California, USA). 1.5× protease and phosphatase inhibitors were subsequently used to maintain phosphorylation status of target proteins. Lysates were clarified by centrifugation and protein concentration determined by Pierce Rapid Gold BCA Assay (Thermo Fisher Scientific, California, USA). 30–50 µg of protein per well was loaded onto 4–20% SurePAGE Bis-Tris gels (GenScript, New Jersey, USA) and separated at 120 V for 1–1.5 hours. Proteins were transferred to either PVDF or nitrocellulose (NC) membranes using iBlot 2 system (Thermo Fisher Scientific, California, USA) and blocked in Tris-buffered saline with 0.1% Tween 20 (TBST) containing 5% non-fat milk or TBST containing 5% bovine serum albumin (BSA) (for phosphoproteins). Membranes were washed and incubated overnight at 4°C with primary antibodies diluted to 1:500–1:1000 in 5% BSA-TBST followed by a 1-hour incubation at room temperature with horseradish peroxidase (HRP)-conjugated

secondary antibodies diluted at 1:2500 in 5% milk-TBST. After washing, membranes were developed with an Immobilon Forte Western HRP substrate (EMD-Millipore, Massachusetts, USA) and imaged on an iBright 1500 Imaging System (Thermo Fisher Scientific, California, USA). For phosphorylated proteins, membranes were first incubated with primary antibodies against specific phosphopeptides; imaged, stripped using Pierce Restore stripping buffer (Thermo Fisher Scientific, California, USA), incubated with primary antibodies against the relevant total protein, and reimaged. Membranes were stripped following image acquisition of target proteins and reprobbed for glyceraldehyde 3-phosphate dehydrogenase (GAPDH) as lysate loading control. Images were exported and densitometry performed using image analysis software ImageJ (National Institutes of Health). Target proteins were normalized to GAPDH as loading control and data presented as fold change from 0 hour. All antibodies used were purchased from Cell Signaling Technologies (Danvers, Massachusetts, USA).

### Statistical analysis

Appropriate statistical analyses were performed in GraphPad Prism (V.9.4). Significance was determined using analysis of variance followed by t-criteria, Mann-Whitney, non-parametric unpaired t-test or independently by Student's t-test with or without Welch's correction, as appropriate. Survival studies were analyzed using the log-rank test. A  $p < 0.05$  was considered statistically significant.

## RESULTS

### IGV-001 elicits T<sub>H</sub>1-polarized tumor-targeting immune responses that control murine GBMs in both preventative and therapeutic settings

To assess the ability of IGV-001 to elicit ICD, we manufactured a mouse (*m*) version of the product based on luciferase-expressing GL261 (GL261-luc2) cells and used it in gold-standard preventative vaccination assays.<sup>28</sup> Specifically, *mIGV-001* or PBS-loaded BDCs were implanted SC in the flank of immunocompetent C57BL/6 albino mice, left in place for 48 hours and then explanted. Twenty-six days later, mice were challenged intracranially with live GL261-luc2 cells (figure 1A). Representative bioluminescence images show development of progressive GBM in mice receiving PBS-loaded BDCs (figure 1B). Conversely, earlier bioluminescence (BLI) readouts (until day 28) demonstrate tumor regression in 47% of mice receiving *mIGV-001* in the preventative setting (figure 1B,C). Mice in the control group had a median OS of 21 days versus 53.5 in *mIGV-001*-exposed mice (figure 1D), pointing to elicitation of protective GBM-targeting immunity. Consistent with this observation, depletion of CD8<sup>+</sup> and more so CD4<sup>+</sup> T cells limited ability of *mIGV-001* to induce preventative immunity in this model (figure 1E). A similar preventative activity was demonstrated harnessing luciferase-expressing mouse hepatocellular carcinoma (HCC) Hepa 1-6(Z1)-luc (hereinafter Hepa 1-6) cells

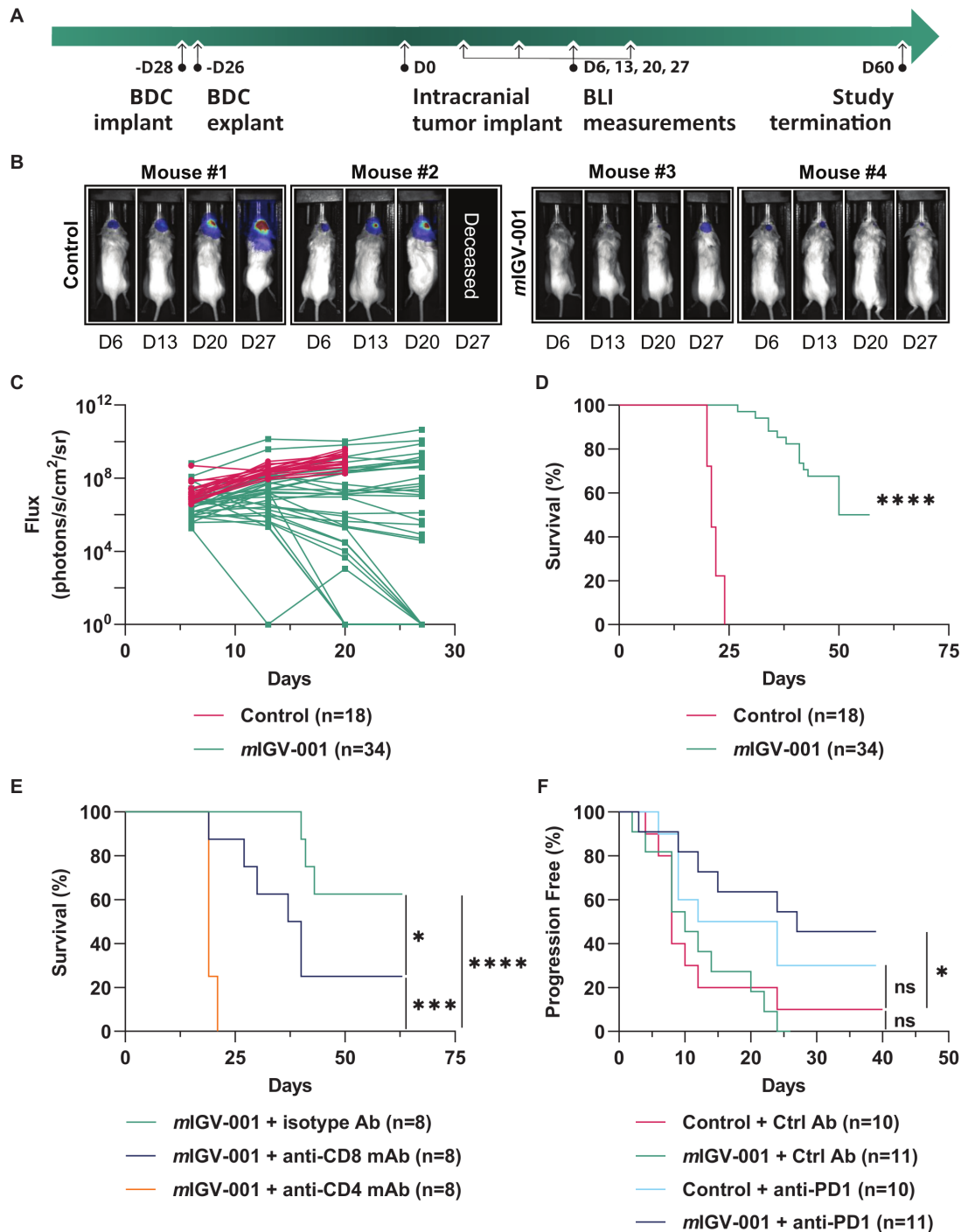


**Figure 1** Mice receiving IGV-001 experienced significantly longer survival or progression-free survival after intracranial tumor challenge with GL261-luc2 cells. Mice were exposed to either *mIGV-001* (manufactured with  $1 \times 10^6$  GL261-luc2 cells/BDC) or PBS-loaded BDC (ie, control). BDCs were implanted in the flank and left in place for 48 hours. Intracranial tumor challenge was performed 26 days after BDC explantation. In the treatment setting, mice received intracranial tumor challenge and 7 days later were randomized into four different groups: (1) PBS-loaded BDC (ie, control) + control Ab; (2) *mIGV-001* + control Ab; (3) PBS-loaded BDC (ie, control) + anti-PD-1 Ab; (4) *mIGV-001*+anti-PD-1 Ab. A BLI flux of  $3.77 \times 10^8$  photons/s/cm<sup>2</sup>/sr was chosen to evaluate time to progression because this value was close to the lethal signal for the majority of the study animals that showed disease progression in the evaluation. (A) BDC treatment schedule and BLI measurement time points for the preventative setting model. (B) Representative bioluminescence images. (C) Individual mice bioluminescence signal (background subtracted) showing reduced tumor burden in most mice receiving *mIGV-001*. (D) Kaplan-Meier survival curves. Median overall survival for control mice=21 days versus 53.5 for mice receiving *mIGV-001*. Log-rank test hazard ratio (HR) of control to *mIGV-001*=7.57 (95% CI 2.757 to 7.57) \*\*\*\* $p < 0.0001$ . (E) Effect of CD4<sup>+</sup> and CD8<sup>+</sup> T-cell depletion in the antitumor responses driven by *mIGV-001*. Log-rank test, \* $p < 0.05$ , \*\*\* $p < 0.001$  \*\*\*\* $p < 0.0001$ . (F) Progression-free survival (%). Log-rank test, \* $p < 0.05$ , ns=not significant. Days=days post-intracranial tumor challenge. n=number of mice. Ab, antibody; BDCs, biodiffusion chambers; BLI, bioluminescent imaging; PBS, phosphate buffered saline; PD-1, programmed cell death 1.

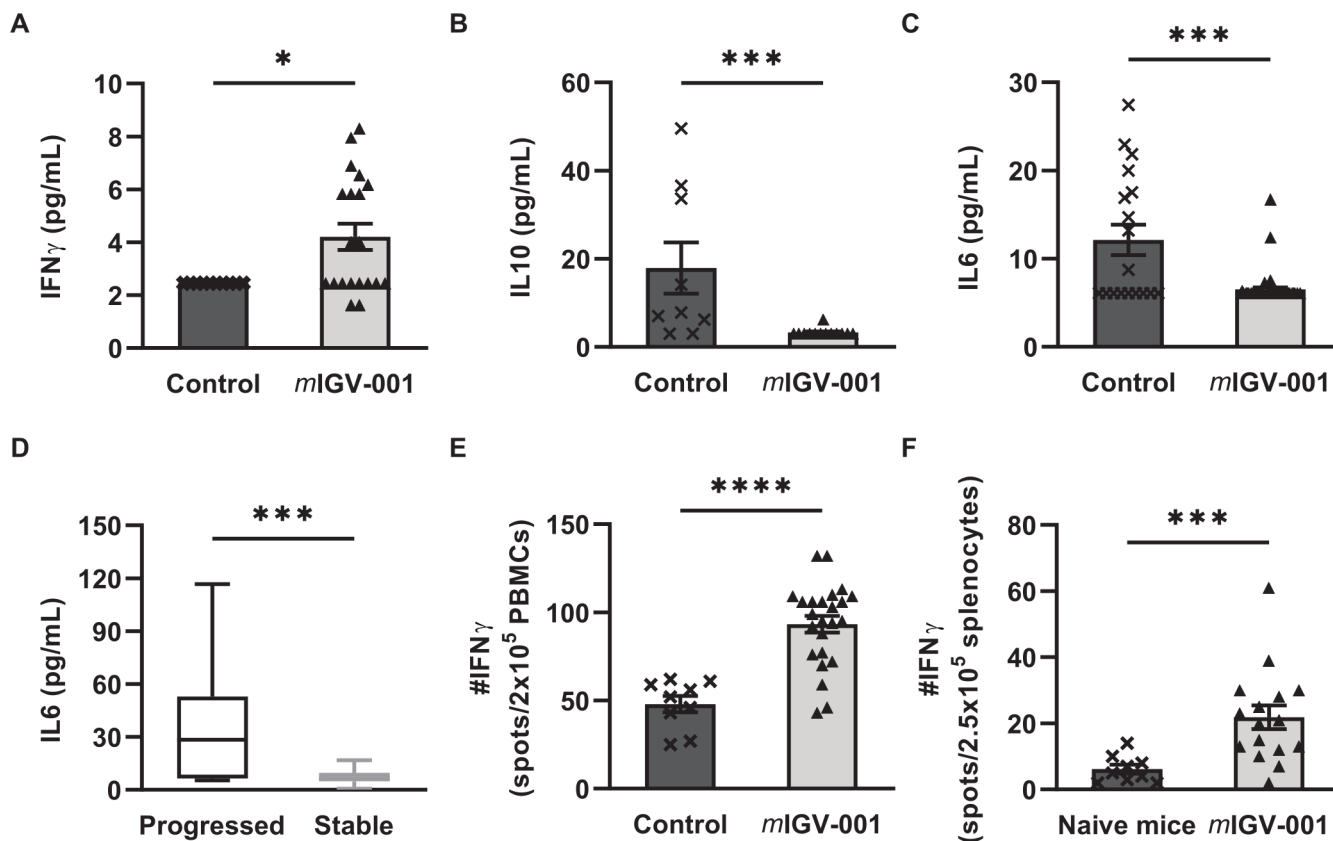


**Figure 2** Preventative treatment with IGV-001 elicits increases in IFN- $\gamma$  coupled to reductions in circulating IL-6 and IL-10. Mice were exposed to either *mIGV-001* (manufactured with  $1 \times 10^6$  GL261-luc2 cells/BDC) or PBS-loaded BDC (ie, control). BDCs were implanted in the flank and left in place for 48 hours. Intracranial tumor challenge was performed 26 days after BDC explantation. Blood samples were collected on days 1, 14, and 28 or when possible, before animals reached ethical abortion criteria (end-of-life). Circulating cytokine levels evaluated in blood samples taken at end-of-life: (A) IFN- $\gamma$  (B) IL-10. (C) IL-6. (D) Circulating levels of IL-6 evaluated on days 1, 14, and 28 days and correlated with BLI measurements on days 6, 13, and 27. At each time point and for each mouse receiving *mIGV-001* ( $n=34$ ), the IL-6 level was assigned to “Progressed” or “Stable” if  $\text{Ln}(\text{BLI total flux}) > 20$  or  $\text{Ln}(\text{BLI total flux}) < 20$ , respectively. (E) IFN- $\gamma$  production by peripheral blood mononuclear cells (collected on day 1) stimulated with tumor lysate-pulsed dendritic cells (controls  $n=3$ , *mIGV-001*  $n=8$ ). (F) IFN- $\gamma$  production by splenocytes (collected on day 28) incubated with major histocompatibility complex-I H-2Db and H-2Kb GL261-specific peptides (naïve=3, *mIGV-001*=6). Results for A–C are presented as mean  $\pm$  SEM from  $n=10$  to 20 mice per group, with individual data points superimposed. Results from D–F are presented mean  $\pm$  SEM of annotated number of mice. Statistical analyses were conducted using Mann-Whitney, non-parametric unpaired t-test. \*\*\*\* $p < 0.0001$ , \*\*\* $p < 0.001$ , \*\* $p < 0.01$ , \* $p < 0.05$ . Ln, natural logarithm; IFN, interferon; IL, interleukin; BDCs, biodiffusion chambers; BLI, bioluminescent imaging; PBS, phosphate buffered saline.

for product manufacturing (online supplemental figure 1A,B). Of note, all mice successfully rejecting orthotopically implanted Hepa 1-6 cells on vaccination, remained fully protected against a second SC inoculation of Hepa 1-6 cells >100 days after initial challenge (online supplemental figure 1C). Importantly, while neither *mIGV-001* nor a PD-1 blocker significantly delayed progression in mice with established GBM, their combination exhibited at least some degree of activity (figure 1F).

Blood samples from mice vaccinated with PBS-loaded BDCs or *mIGV-001* were profiled for multiple  $T_H1$  and  $T_H2$  cytokines at end-of-life. Consistent with the activation of a  $T_H1$  response, IFN- $\gamma$  was elevated while both IL-6 and IL-10 were reduced in sera of mice receiving *mIGV-001*, as compared with their control counterparts (figure 2A–C). Moreover, circulating levels of IL-6 were higher in mice that received *mIGV-001* but developed progressive GBM

as compared with mice actively controlling disease establishment and progression (figure 2D). Finally, T cells isolated from mice receiving *mIGV-001* efficiently responded with IFN- $\gamma$  secretion (as assessed in ELISpot assays) to GL261-luc2 cell lysates (figure 2E) or known GL261-derived MHC class I immunogenic peptides<sup>27</sup> (figure 2F), as compared with T cells from mice receiving PBS-loaded BDCs or naïve mice, respectively.

Taken together, these findings suggest that IGV-001 elicits  $T_H1$ -polarized immunity against GBM cells, which is associated with disease control in mice.

#### IGV-001-draining lymph nodes are enriched in mature antigen-presenting cells and lymphoid effector cells

To elucidate cellular mechanisms involved in preventative GBM-targeting immunity elicited by IGV-001, we used multiparametric flow cytometry to compare



*m*IGV-001-draining lymph nodes (IDLNs) to contralateral lymph nodes (CLNs). IDLNs contained a similar fraction of CD45<sup>+</sup>CD11b<sup>+</sup> myeloid cells as compared with CLNs (figure 3A) but were enriched in CD11c<sup>+</sup>MHC-II<sup>+</sup> DCs (figure 3A), which are involved in antigen presentation.<sup>18</sup> In agreement with these results, IDLNs also contained an increased proportion of CD8<sup>+</sup> and effector CD4<sup>+</sup>FOXP3<sup>-</sup> T cells as compared with CLNs (figure 3B), and both these cellular compartments exhibited a more pronounced polarization towards an effector memory (CD62L<sup>-</sup>CD44<sup>+</sup>) over central memory (CD62L<sup>+</sup>CD44<sup>+</sup>) phenotype (figure 3C,D). Finally, both CD8<sup>+</sup> and effector CD4<sup>+</sup> T cells found in IDLNs were characterized by increased levels of PD-1, as compared with their CLN-resident counterparts (figure 3E).

To extend these findings to an *in vitro* model of immune activation, we used immortalized immature murine DCs (JAWSII cells) to evaluate the expression of maturation markers on co-culture with *m*IGV-001. Specifically, JAWSII cells were pretreated overnight with 100 ng/mL lipopolysaccharide (LPS, a broad DC activatory stimulus) and then either left untreated or exposed for 24 hours to *m*IGV-001 or *m*IGV-001 prepared with paraformaldehyde (PFA)-fixed GL261 cells (which prevents cells from delivering antigenic and immunostimulatory payloads to DCs). In line with *in vivo* data (figure 3A), *m*IGV-001 (but not its PFA-fixed variant) efficiently boosted LPS-driven upregulation of DC activation markers, including CD80, CD86 and MHC-II by JAWSII cells (online supplemental figure 2). Additionally, particle analysis confirmed that during 48 hours *in vitro* incubation, a human (*h*) variant of IGV-001 prepared with T98G human GBM cells produced particles that can efficiently diffuse through the BDC membranes (<0.1 μm) (online supplemental figure 3A). Computational diffusion models generated under static and dynamic conditions demonstrate that regardless of internal concentration, particles of 25–90 nm can exit BDCs. Under static conditions, particle equilibrium inside and outside BDCs could be achieved after 40 hours, 80 hours, and 260 hours for 25 nm, 50 nm and 90 nm particles, respectively (online supplemental figure 3B). Under dynamic conditions, equilibrium was predicted in less than 5 hours, irrespective of particle size (online supplemental figure 3C).

These findings indicate that tumor particles generated by IGV-001 support DC activation in IDLNs, culminating with nodal T-cell expansion and acquisition of effector functions.

### IGV-001 generates ICD-associated danger signals in both mouse and human systems

To characterize immunostimulatory factors underlying the ability of IGV-001 to drive anticancer immunity, we used both *m*IGV-001 and *h*IGV-001 prepared with human T98G or U87 GBM cells. First, we employed multiparametric flow cytometry to assess cytotoxic responses in *m*IGV-001 and *h*IGV-001, and found a statistically significant, time-dependent decrease in recoverable viable cells

(figure 4A). Importantly, similar results were obtained with *h*IGV-001 prepared with patient-derived primary GBM cells and maintained *in vitro* (figure 4B), as well as with both *m*IGV-001 and *h*IGV-001 implanted SC for 48 hours in immunocompetent mice and then explanted (figure 4C). Besides radiation-elicited cellular stress, the demise of GBM cells manipulated to manufacture IGV-001 involves lack of substrate attachment (Online supplemental figure 4A) as well as reduced glucose and protein availability (online supplemental figure 4B–E) within BDCs.

*In vitro*, IGV-001-associated RCD was not accompanied by increased exposure of the “eat-me” signal calreticulin<sup>22</sup> on the surface of GBM cells (online supplemental figure 5). Conversely, IGV-001 elicited RCD along with release of the ICD-associated endogenous immunostimulatory molecule HMGB1<sup>22</sup> in both mouse and human systems, both within BDCs and in the surrounding culture medium (figure 5A,B). Importantly, similar results were obtained not only with *m*IGV-001 and *h*IGV-001 implanted in C57BL/6 mice, as described above (figure 5C), but also in supernatants of BDCs explanted from patients involved in clinical IGV-001 testing (NCT02507583)<sup>16</sup> (figure 5D), which had detectable levels above controls (ie, *in vitro* cultured saline BDCs and surrounding media) and reported circulating levels of HMGB1 in healthy individuals.<sup>29</sup> eATP, another immunostimulatory signal associated with ICD,<sup>22</sup> could also be detected within *m*IGV-001 and *h*IGV-001 BDCs explanted 48 hours after establishment in C57BL/6 mice, respectively (figure 5E). Similarly, eATP was measurable upon *m*IGV-001 and *h*IGV-001 manufacturing *in vitro* (figure 5F), but less so within BDCs (figure 5G–I), potentially reflecting a steep gradient linked to expression of various ectonucleotidases by GBM cells.<sup>30,31</sup>

These data demonstrate the ability of IGV-001 to elicit RCD along with the emission of ICD-associated immunostimulatory signals in both human and mouse GBM models.

### IGV-001 imposes oxidative and endoplasmic reticulum stress onto GBM cells

Next, we investigated the implication of stress response pathways that have previously been linked to the emission of ICD-associated danger signals, such as the integrated stress response (ISR),<sup>22</sup> in immunostimulatory effects of IGV-001. The conditions experienced by GL261 cells in *m*IGV-001 were found to elicit ROS overproduction that could be scavenged, at least partially, by the antioxidant NAC (figure 6A,B). Similar results were observed with *h*IGV-001 (figure 6B). ROS as elicited by *m*IGV-001 manufacturing also turned out to contribute, at least kinetically, to *m*IGV-001-driven cytotoxicity, as demonstrated by cytofluorometric assessment of RCD in the optional presence of NAC (figure 6C). In the human system, though, ROS scavenging failed to alter cytotoxic responses of GBM cells to *h*IGV-001 preparation (figure 6C). *m*IGV-001 resulted in inactivating phosphorylation of eukaryotic

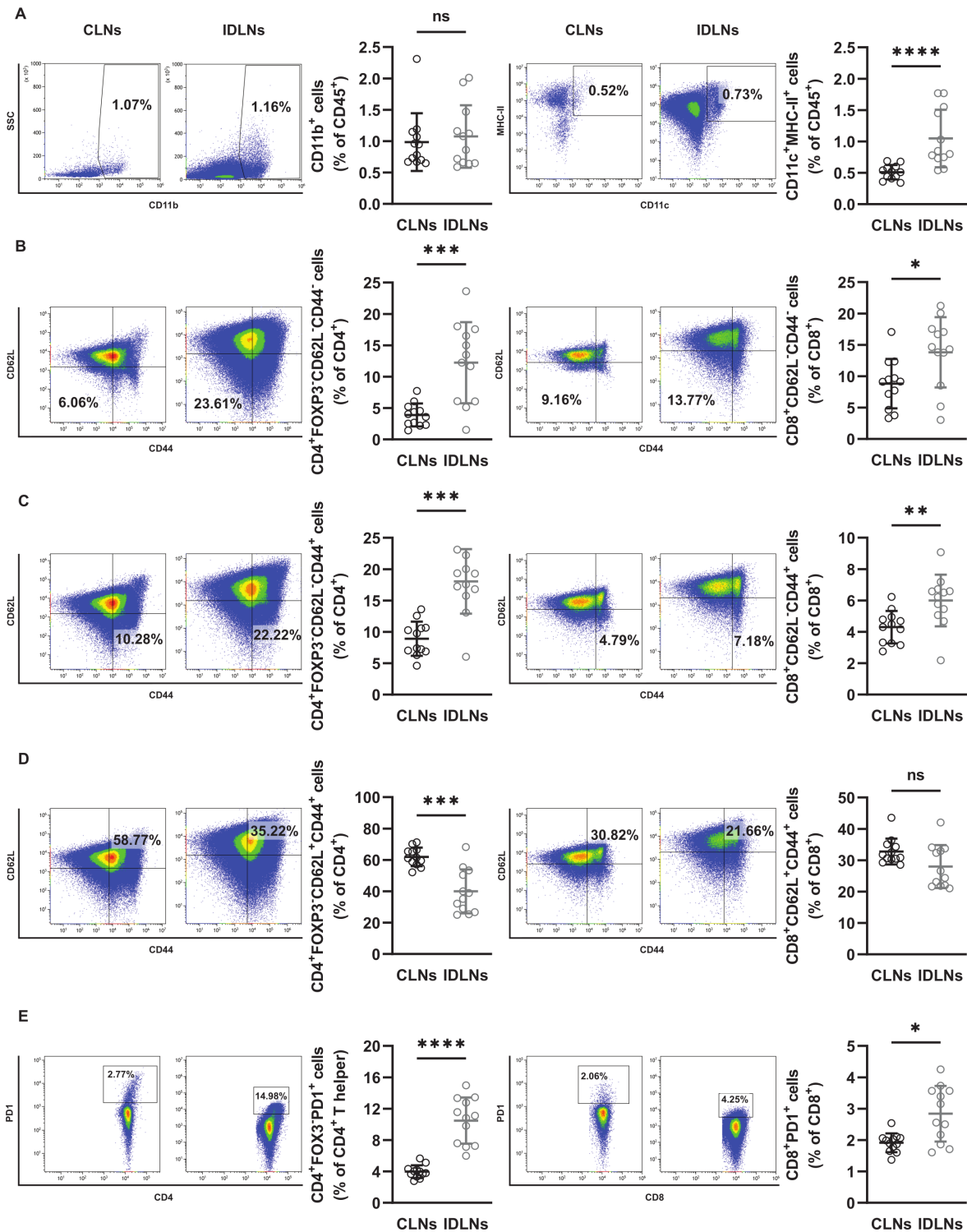


**Figure 3** IGV-001-draining lymph nodes are enriched in mature antigen-presenting cells and lymphoid effector cells. Mice were exposed to *m*IGV-001 (manufactured with  $1 \times 10^6$  GL261-luc2 cells/BDC). BDCs were implanted in the flank and left in place for 48 hours. A subcutaneous tumor challenge with GL261-luc2 ( $1 \times 10^7$  cells/0.2 mL) was performed 26 days after BDC explantation on the same flank, and mice were sacrificed 7 days later. Lymph nodes proximal to the *m*IGV-001 BDCs (IDLNs) and non-draining lymph nodes in the contralateral site (CLNs) were isolated and analyzed by flow cytometry to compare the distribution of myeloid and T-cell subsets. Representative dot plot data and percentages of: (A)  $CD45^+CD11b^+$  myeloid cells and  $CD45^+CD11c^+MHC-II^+$  dendritic cells, (B)  $CD3^+CD4^+FOXP3^-CD62L^-CD44^-$  and  $CD3^+CD8^+CD62L^-CD44^-$  effector T cells, (C)  $CD3^+CD4^+FOXP3^-CD62L^-CD44^+$  and  $CD3^+CD8^+CD62L^-CD44^+$  effector memory T cells, (D)  $CD3^+CD4^+FOXP3^-CD62L^+CD44^+$  and  $CD3^+CD8^+CD62L^+CD44^+$  central memory T cells. (E) PD-1 expression on  $CD4^+$  and  $CD8^+$  T cells. Results are presented as mean  $\pm$  SD of  $n=12$  mice per group. Statistical analysis was performed using unpaired t-test \*\*\*\* $p < 0.0001$ , \*\*\* $p < 0.001$ , \*\* $p < 0.01$ , \* $p < 0.05$ . BDCs, biodiffusion chambers; CLNs, contralateral lymph nodes; IDLNs, draining lymph nodes; MHC, major histocompatibility complex; PD-1, programmed cell death 1.

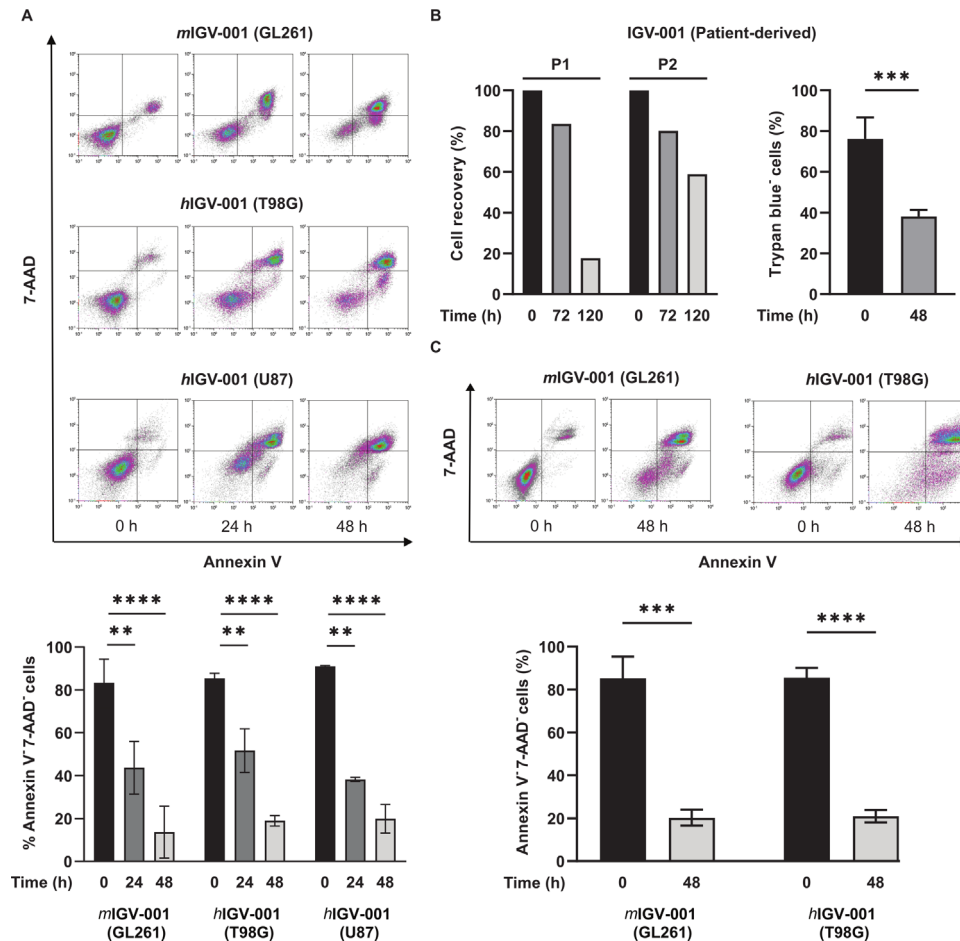


**Figure 4** GBM cells in IGV-001 undergo extensive and time-dependent cell death. *mIGV-001* or *hIGV-001* were prepared and cultured for 24 or 48 hours or retrieved after the 48 hours implantation period in mice. Recovered cells were counted via trypan blue exclusion and evaluated by flow cytometric analysis for annexin V and 7-AAD positivity. (A) Representative dot plots and viability quantification of *mIGV-001* (GL261), *hIGV-001* (T98G), and *hIGV-001* (U87) cells recovered from cultured BDCs. (B) Cell recovery and viability in IGV-001 (manufactured with patient-derived GBM cells). (C) Representative dot plots and viability quantification of *mIGV-001* or *hIGV-001* (T98G) cells recovered from explanted BDCs. Control=phosphate buffered saline or saline filled BDC. Results are presented as mean±SD of two to three independent experiments (or patient samples) with two to three BDCs per condition. Statistical analysis was performed using one-way analysis of variance with multiple comparisons or Welch's t-test, \* $p < 0.05$ , \*\* $p < 0.01$ , \*\*\* $p < 0.001$ , \*\*\*\* $p < 0.0001$ . BDCs, biodiffusion chambers; GBM, glioblastoma.

translation initiation factor 2 subunit alpha (best known as eIF2 $\alpha$ ) (figure 6D), a conserved marker of ISR initiation,<sup>32</sup> coupled with upregulation of ISR effector molecules including activating transcription factor 4 and DNA damage inducible transcript 3 (DDIT3, best known as CHOP)<sup>33</sup> (figure 6E). Moreover, consistent with establishment of oxidative and endoplasmic reticulum stress, we detected rapid phosphorylation of ROS-sensitive kinase mitogen-activated protein kinase 8 (MAPK8, best known as JNK) in GL261 cells manufactured to generate *mIGV-001* (figure 6F).

These findings identify oxidative stress responses and ISR as ICD-associated pathways triggered by IGV-001.

### Molecular RCD mechanisms triggered by IGV-001

Next, we looked at various biomarkers of cell death pathways that have been previously associated with immunogenicity, including apoptotic and necroptotic cell death.<sup>22</sup> Due to the upregulation of CHOP and the

phosphorylation of JNK detected in GL261 cells employed for *mIGV-001* manufacturing (figure 6E,F), we initially focused on apoptotic signaling. Using flow cytometry on staining with dedicated fluorescent markers, we detected a considerable increase in the activity of apoptotic 'executioners' caspase 3 and caspase 7 24 hours after product manufacturing (figure 7A). This was paralleled by an increase in cells with dissipated mitochondrial transmembrane potential ( $\Delta\Psi_m$ ) as well as by the downregulation of the antiapoptotic protein BCL2 apoptosis regulator (BCL2) (figure 7B,C), strongly implicating mitochondrial apoptosis in the cytotoxic effects of *mIGV-001*.<sup>21</sup> Interestingly, however, the necroptotic signal transducer mixed lineage kinase domain like pseudokinase (MLKL) also appeared to undergo activating phosphorylation in the context of *mIGV-001* (figure 7D), potentially suggesting the concomitant activation of multiple RCD pathway by this drug-device product. At least in part supporting

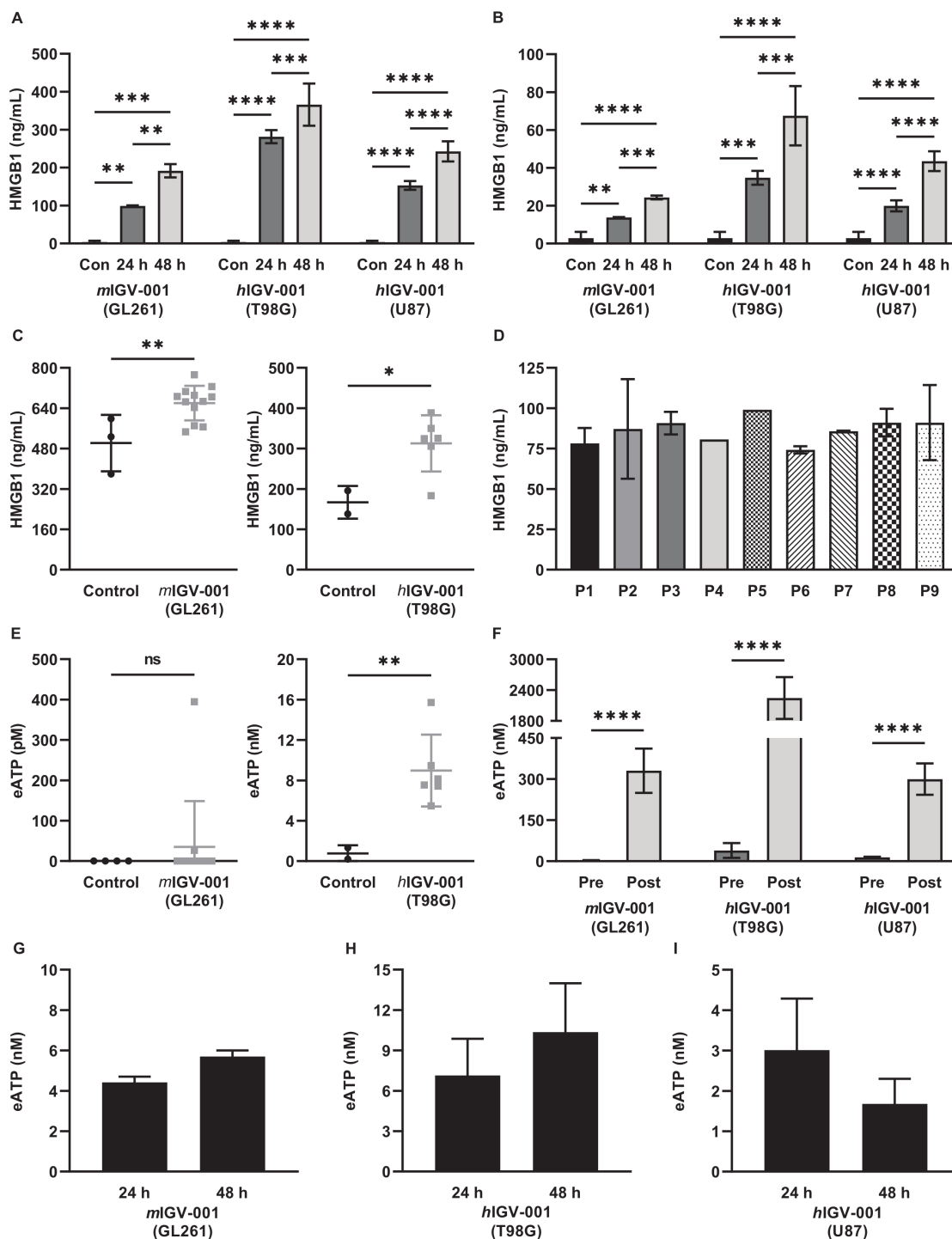


**Figure 5** IGTV-001 generates immunogenic cell death-associated danger signals in both mouse and human systems. *m*IGV-001 or *h*IGV-001 (prepared with U97 or T98G cells) were manufactured and cultured for 24 or 48 hours or retrieved after the 48 hours implantation period in mice. HMGB1 was evaluated by ELISA and ATP content was measured using RealTime-Glo extracellular ATP assay. HMGB1 levels: (A) within *m*IGV-001 or *h*IGV-001 BDCs cultured in vitro and (B) in the surrounding media. (C) HMGB1 measured in *m*IGV-001 or *h*IGV-001 BDCs explanted from mice. (D) HMGB1 measured in recovered BDCs from patients enrolled in NCT02507583. (E) eATP measured in *m*IGV-001 or *h*IGV-001 BDCs explanted from mice. (F) eATP measured in *m*IGV-001 or *h*IGV-001 after manufacturing and prior to loading into BDCs. eATP measured in (G) *m*IGV-001 (GL261), (H) *h*IGV-001 (T98G), and (I) *h*IGV-001 (U87) BDCs supernatants. Con=phosphate buffered saline or saline filled BDC. Pre=pre-manufacturing; post=post-manufacturing (or at time 0 hour). Patient samples (P#) were selected based on sample availability and results are presented as mean±SD of two technical replicates. In vitro data are presented as mean±SD of two to three independent experiments with two to three BDCs per condition. In vivo data are presented as mean±SD of 12 or six independent BDCs for *m*IGV-001 and *h*IGV-001, respectively. Statistical analysis was performed using one-way analysis of variance with multiple comparisons or Welch's t-test, \* $p < 0.05$ , \*\* $p < 0.01$ , \*\*\* $p < 0.001$ , \*\*\*\* $p < 0.0001$ . BDCs, biodiffusion chambers; eATP, extracellular ATP; HMGB1, high mobility group box 1.

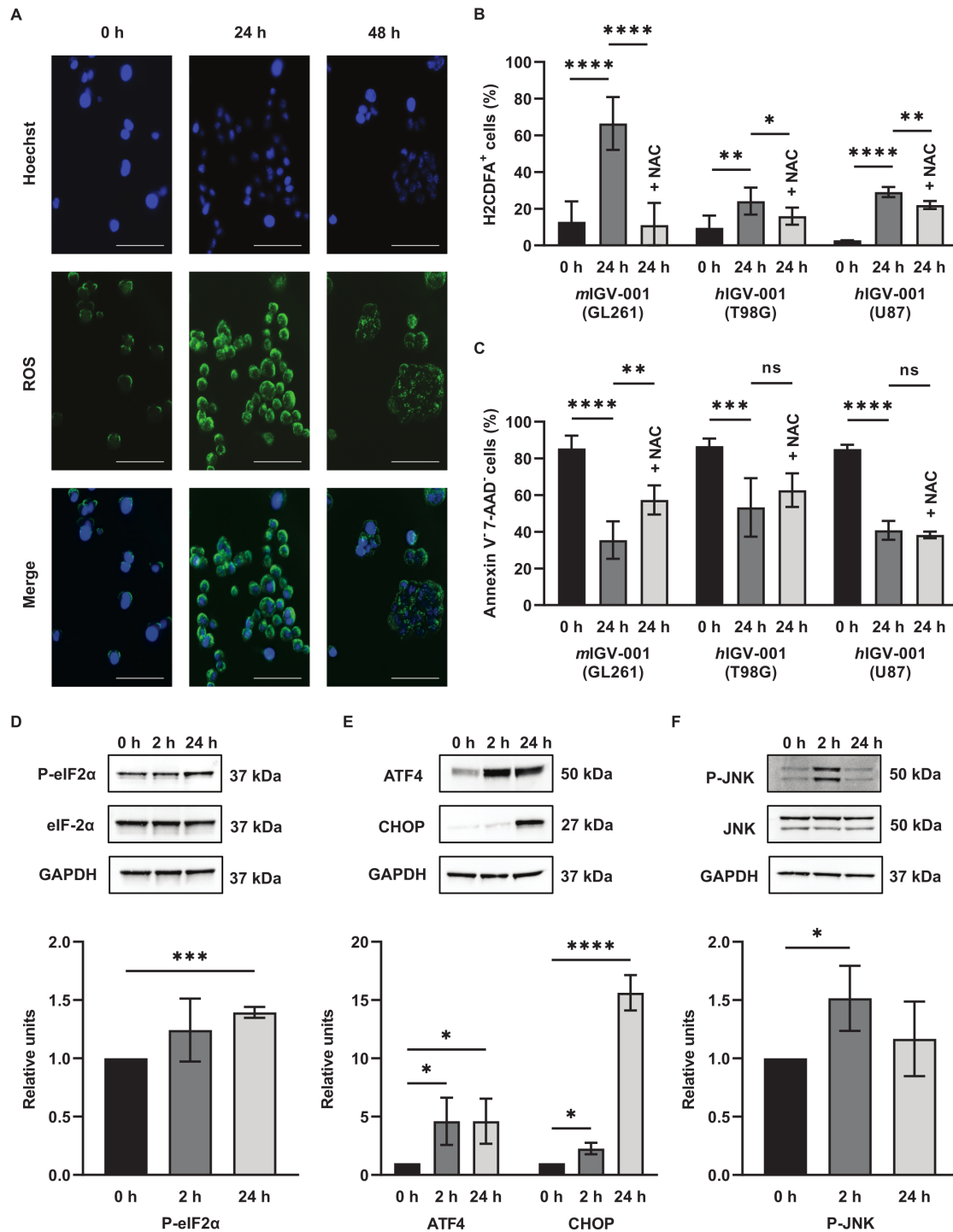


**Figure 6** IGTV-001 imposes oxidative and ER stress on GBM cells in vitro. *mlGV-001* was manufactured and cultured for 24 hours. To quantify oxidative stress, cells were retrieved from the BDCs and stained with dye and analyzed via flow cytometry or imaged using fluorescence microscopy. Where indicated, cultures were treated with N-acetyl cysteine (NAC; 1 or 2 mM). In separate experiments, retrieved cells were used for immunoblotting to detect ER stress markers. (A) Representative fluorescence microscopy images of ROS accumulation within *mlGV-001* GBM cells. (B) Flow cytometric quantification of ROS accumulation in *mlGV-001* or *hIGV-001* with (C) corresponding cell viability in the presence of the ROS scavenger, NAC. Western blot analyses of integrated stress response markers (D) eIF2 $\alpha$ , (E) ATF4 and CHOP. (F) Activation of the ROS-sensitive effector kinase JNK. Western blot images are representative of one experiment out of three independent runs. Average normalized band densitometry for eIF2 $\alpha$ , ATF4, and CHOP are plotted below the corresponding images. Results are presented as mean $\pm$ SD of three independent experiments with two to three BDCs per condition. Magnification=40 $\times$ . Scale bar=75 $\mu$ m. Statistical analysis was performed using either standard unpaired or Welch's corrected t-test, \* $p$ <0.05, \*\* $p$ <0.01, \*\*\* $p$ <0.001, \*\*\*\* $p$ <0.0001. ATF4, activating transcription factor 4; BDCs, biodiffusion chambers; CHOP, DNA damage inducible transcript 3; eIF2 $\alpha$ , eukaryotic translation initiation factor 2 subunit alpha; ER, endoplasmic reticulum; GAPDH, glyceraldehyde 3-phosphate dehydrogenase; GBM, glioblastoma; JNK, mitogen-activated protein kinase 8; ROS, reactive oxygen species.

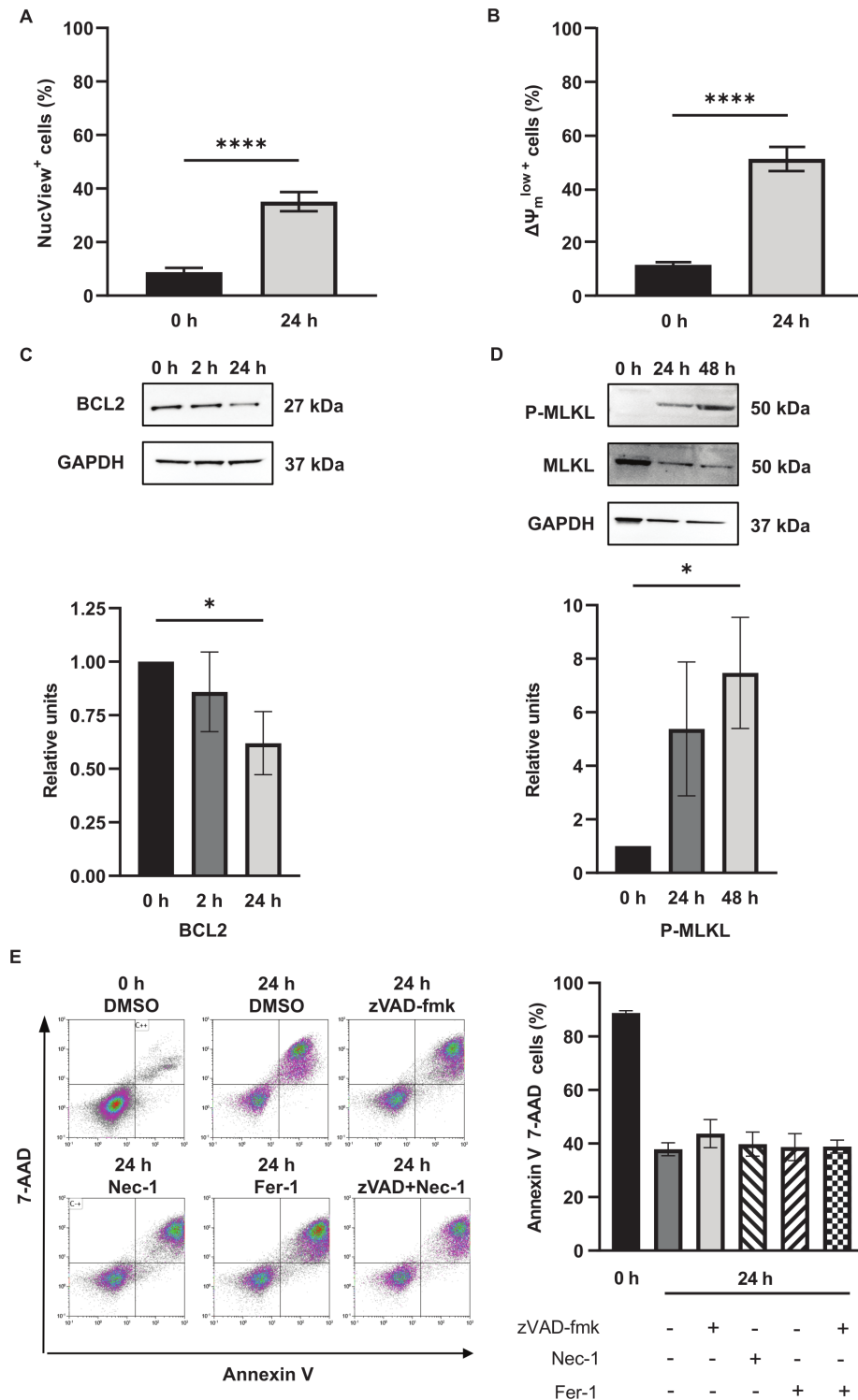


**Figure 7** IGV-001 triggers molecular RCD mechanisms in vitro. *mIGV-001* was manufactured and cultured for 24 hours. Cells retrieved from the biodiffusion chambers were analyzed by flow cytometry to detect apoptotic cell death signaling via caspase 3/7 activity (NucView staining) and changes in mitochondrial membrane potential ( $\Delta\Psi_m$ ). In separate experiments, retrieved cells were used for immunoblotting to detect RCD-associated markers. For cell death inhibition, *mIGV-001* cells were co-incubated with 25  $\mu\text{M}$  zVAD-fmk, 30  $\mu\text{M}$  necrostatin-1 (Nec-1) or 1  $\mu\text{M}$  ferrostatin-1 (Fer-1) and analyzed for viability by flow cytometry (annexin V and 7-AAD staining). (A) Caspase 3/7 activity. (B) Mitochondrial membrane potential. Western blot analyses of (C) the anti-apoptotic effector BCL2 and (D) the necroptotic signal transducer P-MLKL. (E) Representative dot plots and viability quantification on cell death inhibition. Western blot images are representative of one experiment out of three independent runs. Average normalized band densitometry for BCL2 and P-MLKL are plotted below the corresponding images. Statistical analysis was performed using either standard unpaired or Welch's corrected t-test, \* $p < 0.05$ , \*\* $p < 0.01$ , \*\*\* $p < 0.001$ , \*\*\*\* $p < 0.0001$ . DMSO, dimethyl sulfoxide; GAPDH, glyceraldehyde 3-phosphate dehydrogenase; MLKL, mixed lineage domain like pseudokinase; RCD, regulated cell death.

this result, pharmacological inhibition of apoptosis with the pan-caspase blocker zVAD-fmk, necroptosis with the receptor interacting serine/threonine kinase 1 (RIPK1) inhibitor Nec-1, or ferroptosis (another regulated variant of necrosis) with Fer-1 did not alter the kinetic of RCD as imposed on GL261 cells by *m*IGV-001 manufacturing (figure 7E).

These findings suggest that IGV-001 immunogenicity may originate from the activation of a multipronged RCD program downstream of failing adaptation to stress.

## DISCUSSION

Taken together, the findings reported herein demonstrate that IGV-001 elicits immunogenic cellular stress culminating with *bona fide* ICD and the activation of therapeutically relevant,  $T_H1$ -polarized immune responses against GBM. These data are in line with immunological correlates measured in patients with newly diagnosed GBM receiving IGV-001 as part of a recently reported Phase 1b clinical trial.<sup>16</sup> Specifically, peak elevations of circulating IFN- $\gamma$ , IL-2, and IL-12, which altogether reflect DC maturation culminating with T-cell activation/expansion,<sup>18</sup> were observed shortly after IGV-001 implantation to patients with GBM.<sup>16</sup> While these changes did not persist systemically over time, most likely owing to the immunosuppressive nature of SOC therapy delivered to all patients involved in this study,<sup>34</sup> they suggest that IGV-001-driven ICD may also be operational in patients with GBM.

Interestingly, the ability of IGV-001-driven ICD to protect mice from a subsequent challenge with GBM cells was compromised on depletion of CD8<sup>+</sup> or CD4<sup>+</sup> T cells, which is in line not only with the need of both these cell compartments for ICD to mount optimal tumor-targeting responses,<sup>22</sup> but also with a previously described key role of both CD8<sup>+</sup> and CD4<sup>+</sup> T cells in the control of mouse GBM GL261 cells.<sup>35</sup> However, while we were able to directly assess CD8<sup>+</sup> T-cell reactivity in the periphery of mice receiving IGV-001 on stimulation with GL261 cell-specific MHC class I-restricted peptides, similar MHC class II-restricted reagents are unavailable, which complicated direct assessment. Thus, whether CD4<sup>+</sup> T cells contribute to GBM-targeting immunity as elicited by IGV-001 purely as ‘helpers’ for CD8<sup>+</sup> T cells or also by mediating direct antitumor effects (as reported in multiple other mouse tumor models)<sup>36</sup> remains to be formally validated.

Our findings suggest that IGV-001-elicited immune responses exhibit signs of  $T_H1$  polarization, including decreased circulating IL-6. Importantly, IL-6 has previously been associated with tumor progression in multiple human solid tumors, including GBM.<sup>37</sup> Moreover, tumor-derived IL-6 has previously been found to upregulate the immunosuppressive molecule CD274 (best known as programmed cell death ligand-1; PD-L1) on GBM-infiltrating myeloid cells, culminating with accelerated GBM progression.<sup>38</sup> Consistent with these findings, IL-6 blockade limited intratumoral PD-L1 expression and

improved the survival of GL261-bearing mice.<sup>38</sup> These findings suggest that at least part of the therapeutic effects of IGV-001 may result from reductions in IL-6.

Importantly, GBM generally displays scarce infiltration by immune cells (ie, it is a so-called “cold” tumor) and hence is virtually insensitive to ICIs<sup>9</sup> and other immunotherapeutic agents.<sup>10–12</sup> IGV-001 immunotherapy may be advantageous in this respect as BDCs are implanted at abdominal acceptor sites between the rectus muscle and sheath,<sup>39</sup> which are minimally affected by the immunosuppressive intracranial microenvironment established by progressing GBM.<sup>40</sup>

One of the caveats of this study is predominant reliance on preventative rather than therapeutic experimental settings. This largely reflects our focus on *bona fide* ICD, which can primarily be discerned from RCD-independent immunostimulation in preventative vaccination assays.<sup>28</sup> Indeed, therapeutic models based on systemic interventions cannot readily discriminate against ICD over a direct immunostimulatory effect of the treatment that does not involve RCD.<sup>28</sup> Moreover, established GL261 GBMs are highly aggressive, often enabling insufficient time for the establishment of therapeutically relevant anticancer immunity in therapeutic settings (ie, when treatment is initiated in the presence of detectable tumors). That said, while neither IGV-001 nor a PD-1 blocker employed as standalone agents delayed progression in GBM-bearing mice, the combinatorial regimen elicited at least some degree of tumor control. Whether such a control can be boosted with additional immunotherapeutic agents with proven activity in murine GBM such as tumor necrosis factor receptor superfamily member 4 (TNFRSF4, best known as OX40) agonists<sup>41</sup> remains to be formally elucidated. Irrespective of this caveat, IGV-001 has already shown potential activity in the clinic.<sup>16</sup>

Another limitation of our studies emerges from the use of a C57BL/6 mouse background, as imposed by the GL261 model to preserve a syngeneic system.<sup>42</sup> C57BL/6 mice are indeed intrinsically prone to mount  $T_H1$ -polarized responses as compared with BALB/c mice and other mouse strains,<sup>43</sup> which may not necessarily reflect the natural polarization of tumor-targeting immunity in humans. However, all well-characterized transplantable mouse models of GBMs are syngeneic to C57BL/6 mice,<sup>42</sup> and surgical resection of transgene-driven GBMs (most of which are anyway available in the C57BL/6 mouse background)<sup>42</sup> for individual IGV-001 manufacturing is not technically practical. Novel transplantable mouse models of GBMs syngeneic to BALB/c mice are needed to extend our findings to a different mouse strain.

Finally, it is plausible (although it remains to be formally investigated) that cancer cell type may influence, at least to some degree, the ability of IGV-001 to elicit tumor-targeting immunity downstream of ICD. For instance, it is conceivable that cancer cells with intrinsic defects in ICD-associated stress responses, such as the ISR or autophagy (which underlies ATP release during ICD),<sup>44</sup> may engage suboptimal immunostimulation on

IGV-001 administration. Along similar lines, the impact of tumor mutational burden (TMB), which has been associated with sensitivity to ICIs in multiple cohorts of patients with cancer,<sup>45</sup> on the immunogenicity of IGV-001 remains to be fully assessed. Whether assessing TMB and/or functional markers of a functional ISR or proficient autophagy may identify patients at increased likelihood to respond to IGV-001 remains to be investigated.

Despite these and other caveats, our data formally establish IGV-001 as a *bona fide* ICD inducer in both mouse and human model systems, warranting further preclinical and clinical investigation into IGV-001 in combination with immunotherapy. Moreover, our findings with HCC cells support the utility of this biologic-device platform for the treatment of solid tumors for which malignant cells can be readily isolated, other than GBM. Work is underway to explore and develop a therapeutic platform with broader applications based on the mechanism of action of IGV-001.

#### Author affiliations

<sup>1</sup>Department of Research, Imvax, Inc, Philadelphia, Pennsylvania, USA

<sup>2</sup>Department of Neurosurgery, Thomas Jefferson University, Philadelphia, Pennsylvania, USA

<sup>3</sup>Department of Clinical Operations, Imvax, Inc, Philadelphia, Pennsylvania, USA

<sup>4</sup>CBS Squared, Inc, Philadelphia, Pennsylvania, USA

<sup>5</sup>Department of Radiation Oncology, Weill Cornell Medical College, New York, New York, USA

<sup>6</sup>Sandra and Edward Meyer Cancer Center, New York, New York, USA

<sup>7</sup>Caryl and Israel Englander Institute for Precision Medicine, New York, New York, USA

**Acknowledgements** The authors would like to acknowledge John Limongelli and Drs Raul Perez-Olle and Belen Carrillo-Rivas for their critical review of this manuscript. We would like to thank Ms Mayrimar Torres for her outstanding laboratory management. Finally, we would like to recognize the Preclinical Oncology group at Labcorp Drug Development, the In Vivo Pharmacology group at Reaction Biology, Germany, and the In Vivo Research Services staff at Rutgers University, for their assistance with the execution of in vivo experiments.

**Contributors** CC: Experimental planning, data curation, formal analysis, and writing (original draft). CU: Experimental planning, data curation, formal analysis, and writing (original draft). KK: Data curation, formal analysis. EAE: Data curation. AZ: Data curation. DWA: Writing (review and editing). CS: Statistical analyses. LG: Writing (review and editing). MAE: Investigation, writing (review and editing) and guarantor. JZ: Investigation, experimental planning, conceptualization, formal analysis, writing (original draft, review, and editing).

**Funding** The authors have not declared a specific grant for this research from any funding agency in the public, commercial or not-for-profit sectors.

**Competing interests** CC, CU, KK, EAE, AZ, DWA, MAE, and JZ are/were employed by Imvax. CS is a paid consultant of Imvax. LG is/has been holding research contracts with Lytix Biopharma, Promontory and Onxeo, has received consulting/ advisory honoraria from Boehringer Ingelheim, AstraZeneca, OmniSEQ, Onxeo, The Longevity Labs, Inzen, Imvax, Sofio, Promontory, Noxopharm, EduCom, and the Luke Heller TECPR2 Foundation, and holds Promontory stock options.

**Patient consent for publication** Consent obtained directly from patient(s).

**Ethics approval** There are two institutional review board protocols involved with this study. Please see below for their titles, control# and Board# (153 and 2405). (1) Phase I Study in Humans Evaluating the Safety of Rectus Sheath Implantation of Diffusion Chambers Encapsulating Autologous Malignant Glioma Cells Treated with Insulin Growth Factor Receptor-1 Antisense Oligodeoxynucleotide (IGF-1 R/AS DON) in 32 Patients with Newly Diagnosed Malignant Glioma (Private Foundation) Control #14G.96Document(s) Approved: Clinical Study Protocol 102.0, Study Number: Protocol #TJU-14379-102, Version #102.0 dated 02 Jan 2014; Informed Consent Version V1.0In accordance with Federal-Wide Assurance #00002109 to

the US Department of Health and Human Services, this study was approved by Board #153. (2) Analysis of cell count, viability, and immunogenicity of de-identified discarded newly diagnosed glioblastoma tissue and more broadly other newly diagnosed solid tumor tissues from the operating room. Control #21C.030In accordance with Federal-Wide Assurance #00002109 to the US Department of Health and Human Services, this study was approved by Board #2405. Participants gave informed consent to participate in the study before taking part.

**Provenance and peer review** Not commissioned; externally peer reviewed.

**Data availability statement** Data are available upon reasonable request.

**Supplemental material** This content has been supplied by the author(s). It has not been vetted by BMJ Publishing Group Limited (BMJ) and may not have been peer-reviewed. Any opinions or recommendations discussed are solely those of the author(s) and are not endorsed by BMJ. BMJ disclaims all liability and responsibility arising from any reliance placed on the content. Where the content includes any translated material, BMJ does not warrant the accuracy and reliability of the translations (including but not limited to local regulations, clinical guidelines, terminology, drug names and drug dosages), and is not responsible for any error and/or omissions arising from translation and adaptation or otherwise.

**Open access** This is an open access article distributed in accordance with the Creative Commons Attribution Non Commercial (CC BY-NC 4.0) license, which permits others to distribute, remix, adapt, build upon this work non-commercially, and license their derivative works on different terms, provided the original work is properly cited, appropriate credit is given, any changes made indicated, and the use is non-commercial. See <http://creativecommons.org/licenses/by-nc/4.0/>.

#### ORCID iD

Jenny Zilberberg <http://orcid.org/0000-0002-4139-2616>

#### REFERENCES

- Ostrom QT, Patil N, Cioffi G, *et al*. CBTRUS statistical report: primary brain and other central nervous system tumors diagnosed in the United States in 2013-2017. *Neuro Oncol* 2020;22(12 Suppl 2):iv1-96.
- Stupp R, Mason WP, van den Bent MJ, *et al*. Radiotherapy plus concomitant and adjuvant Temozolomide for glioblastoma. *N Engl J Med* 2005;352:987-96.
- Vitale I, Shema E, Loi S, *et al*. Intratumoral heterogeneity in cancer progression and response to immunotherapy. *Nat Med* 2021;27:212-24.
- DeCordova S, Shastri A, Tsolaki AG, *et al*. Molecular heterogeneity and immunosuppressive Microenvironment in glioblastoma. *Front Immunol* 2020;11:1402.
- Iglesia MD, Parker JS, Hoadley KA, *et al*. Genomic analysis of immune cell infiltrates across 11 tumor types. *J Natl Cancer Inst* 2016;108:djw144.
- Exley MA, Garcia S, Zellander A, *et al*. Challenges and opportunities for immunotherapeutic intervention against myeloid immunosuppression in glioblastoma. *J Clin Med* 2022;11:1069.
- Grabowski MM, Sankey EW, Ryan KJ, *et al*. Immune suppression in gliomas. *J Neurooncol* 2021;151:3-12.
- Fisher JP, Adamson DC. Current FDA-approved therapies for high-grade malignant gliomas. *Biomedicines* 2021;9:324.
- Reardon DA, Brandes AA, Omuro A, *et al*. Effect of Nivolumab vs Bevacizumab in patients with recurrent glioblastoma: the Checkmate 143 phase 3 randomized clinical trial. *JAMA Oncol* 2020;6:1003-10.
- O'Rourke DM, Nasrallah MP, Desai A, *et al*. A single dose of peripherally infused Egrfviii-directed CAR T cells mediates antigen loss and induces adaptive resistance in patients with recurrent glioblastoma. *Sci Transl Med* 2017;9:ea00984.
- Datsi A, Sorg RV. Dendritic cell vaccination of glioblastoma: road to success or dead end. *Front Immunol* 2021;12:770390.
- Curry WT Jr, Gorrepati R, Piesche M, *et al*. Vaccination with irradiated Autologous tumor cells mixed with irradiated GM-K562 cells stimulates antitumor immunity and T lymphocyte activation in patients with recurrent malignant glioma. *Clinical Cancer Research* 2016;22:2885-96.
- Laureano RS, Sprooten J, Vanmeerbeek I, *et al*. Trial watch: Dendritic cell (DC)-Based Immunotherapy for cancer. *Oncoimmunology* 2022;11:2096363.
- Aranda F, Vacchelli E, Eggermont A, *et al*. Trial watch: peptide vaccines in cancer therapy. *Oncoimmunology* 2013;2:e26621.
- Vacchelli E, Vitale I, Eggermont A, *et al*. Trial watch: Dendritic cell-based interventions for cancer therapy. *Oncoimmunology* 2013;2:e25771.



- 16 Andrews DW, Judy KD, Scott CB, *et al.* Phase IB clinical trial of IGV-001 for patients with newly diagnosed glioblastoma. *Clinical Cancer Research* 2021;27:1912–22.
- 17 Zhao L, Zhang S, Kepp O, *et al.* Dendritic cell transfer for cancer Immunotherapy. *Int Rev Cell Mol Biol* 2022;370:33–64.
- 18 Wculek SK, Cueto FJ, Mujal AM, *et al.* Dendritic cells in cancer Immunology and Immunotherapy. *Nat Rev Immunol* 2020;20:7–24.
- 19 Boada-Romero E, Martinez J, Heckmann BL, *et al.* The clearance of dead cells by Efferocytosis. *Nat Rev Mol Cell Biol* 2020;21:398–414.
- 20 Rothlin CV, Hille TD, Ghosh S. Determining the Effector response to cell death. *Nat Rev Immunol* 2021;21:292–304.
- 21 Galluzzi L, Vitale I, Aaronson SA, *et al.* Molecular mechanisms of cell death: recommendations of the nomenclature Committee on cell death 2018. *Cell Death Differ* 2018;25:486–541.
- 22 Kroemer G, Galassi C, Zitvogel L, *et al.* Immunogenic cell stress and death. *Nat Immunol* 2022;23:487–500.
- 23 Galluzzi L, Humeau J, Buqué A, *et al.* Immunostimulation with chemotherapy in the era of immune Checkpoint inhibitors. *Nat Rev Clin Oncol* 2020;17:725–41.
- 24 Petroni G, Buqué A, Zitvogel L, *et al.* Immunomodulation by targeted anticancer agents. *Cancer Cell* 2021;39:310–45.
- 25 Rodriguez-Ruiz ME, Vitale I, Harrington KJ, *et al.* Immunological impact of cell death signaling driven by radiation on the tumor Microenvironment. *Nat Immunol* 2020;21:120–34.
- 26 Tatsuno K, Yamazaki T, Hanlon D, *et al.* Extracorporeal Photochemotherapy induces BONA fide Immunogenic cell death. *Cell Death Dis* 2019;10:578.
- 27 Johanns TM, Ward JP, Miller CA, *et al.* Endogenous Neoantigen-specific Cd8 T cells identified in two glioblastoma models using a cancer Immunogenomics approach. *Cancer Immunology Research* 2016;4:1007–15.
- 28 Galluzzi L, Vitale I, Warren S, *et al.* Consensus guidelines for the definition, detection and interpretation of Immunogenic cell death. *J Immunother Cancer* 2020;8:e000337.
- 29 Rocha DCP, Souza TMA, Nunes PCG, *et al.* Increased circulating levels of high mobility group box 1 (Hmgb1) in acute-phase Chikungunya virus infection: potential disease biomarker. *J Clin Virol* 2022;146:105054.
- 30 Scheffel TB, Rockenbach L, Cruz FF, *et al.* Inhibition of ATP hydrolysis as a key regulator of Temozolomide resistance and migratory phenotype of glioblastoma cells. *Biochem Biophys Res Commun* 2022;601:24–30.
- 31 Wang M, Jia J, Cui Y, *et al.* Cd73-positive extracellular Vesicles promote glioblastoma immunosuppression by inhibiting T-cell Clonal expansion. *Cell Death Dis* 2021;12:1065.
- 32 Bezu L, Humeau J, Leduc M, *et al.* Assessment of Eif2A Phosphorylation during Immunogenic cell death. *Methods Cell Biol* 2022;172:83–98.
- 33 Hetz C. The unfolded protein response: controlling cell fate decisions under ER stress and beyond. *Nat Rev Mol Cell Biol* 2012;13:89–102.
- 34 Bae SH, Park M-J, Lee MM, *et al.* Toxicity profile of Temozolomide in the treatment of 300 malignant glioma patients in Korea. *J Korean Med Sci* 2014;29:980–4.
- 35 Khan SM, Desai R, Coxon A, *et al.* Impact of Cd4 T cells on Intratumoral Cd8 T-cell exhaustion and responsiveness to PD-1 blockade therapy in Mouse brain tumors. *J Immunother Cancer* 2022;10:e005293.
- 36 Lhuillier C, Rudqvist N-P, Yamazaki T, *et al.* Radiotherapy-exposed Cd8+ and Cd4+ neoantigens enhance tumor control. *J Clin Invest* 2021;131:e138740.
- 37 Yeung YT, McDonald KL, Grewal T, *et al.* Interleukins in glioblastoma pathophysiology: implications for therapy. *Br J Pharmacol* 2013;168:591–606.
- 38 Lamano JB, Lamano JB, Li YD, *et al.* Glioblastoma-derived Il6 induces immunosuppressive peripheral myeloid cell PD-L1 and promotes tumor growth. *Clinical Cancer Research* 2019;25:3643–57.
- 39 Andrews DW, Resnicoff M, Flanders AE, *et al.* Results of a pilot study involving the use of an Antisense Oligodeoxynucleotide directed against the insulin-like growth factor type I receptor in malignant Astrocytomas. *J Clin Oncol* 2001;19:2189–200.
- 40 Zhang X, Zhao L, Zhang H, *et al.* The immunosuppressive Microenvironment and Immunotherapy in human glioblastoma. *Front Immunol* 2022;13:1003651.
- 41 Jahan N, Talat H, Alonso A, *et al.* Triple combination Immunotherapy with GVAX, anti-PD-1 Monoclonal antibody, and agonist anti-Ox40 Monoclonal antibody is highly effective against murine intracranial glioma. *Oncimmunology* 2019;8:e1577108.
- 42 Haddad AF, Young JS, Amara D, *et al.* Mouse models of glioblastoma for the evaluation of novel therapeutic strategies. *Neurooncol Adv* 2021;3:vdab100.
- 43 Watanabe H, Numata K, Ito T, *et al.* Innate immune response in Th1- and Th2-dominant Mouse strains. *Shock* 2004;22:460–6.
- 44 Kepp O, Bezu L, Yamazaki T, *et al.* ATP and cancer Immunosurveillance. *EMBO J* 2021;40:e108130.
- 45 Alban TJ, Chan TA. Immunotherapy biomarkers: the long and winding road. *Nat Rev Clin Oncol* 2021;18:323–4.

## Supplemental Materials and Methods

### *Maturation of dendritic cells*

JAWSII cells were pretreated with 100 ng/ml LPS for ~18 h prior to co-culturing with either 10 µg/ml LPS, *mIGV-001*, or *mIGV-001* prepared with fixed cells for 24 h at 37°C under 5% CO<sub>2</sub>. To prevent cellular debris from forming and diffusing out of the BDC, *mIGV-001* was also manufactured with fixed with 4% paraformaldehyde prior to loading into the BDC. After 24 h JAWSII cells were harvested and resuspended in PBS + 5% FBS containing antibodies (Miltenyi Biotech, Germany) for CD80 (130-116-395), CD86 (130-123-279), CD11b (130-113-811), CD11c (130-110-701), and MHCII (130-112-234) and incubated for 30 minutes at RT in the dark. Stained cells were washed and then analyzed on a MACSQuant Analyzer 16 flow cytometer. Data analysis was performed using the Kaluza Analysis Software and presented as a fold increase compared to unstimulated JAWSII cells.

### *Computational models of nanoparticle transport*

Particle concentration in the supernatant of *hIGV-001* (T98G) after *in vitro* culture for 48 h was analyzed on a Malver NanoSight NS300 nanoparticle tracking analysis (NTA) instrument by The Particle Technology Labs (Downers Grove, IL). Nanoparticle transport was modeled using the Kedem-Katchalsky system of equations governing solute transport kinetics across semi-permeable membranes in MATLAB 2022a (Mathworks™). Briefly, an ordinary differential equation solver (ODE45) in MATLAB was utilized to solve the Kedem-Katchalsky system of

equations operating under specific system starting conditions in order to obtain the concentration of nanoparticles present outside of the BDC. Nanoparticle transport was modeled under passive (pure diffusion) and actively driven (driving fluid flow) conditions. Initial starting conditions for the system under passive transport conditions were set as follows: Nanoparticle diameters = 25, 50 & 90 nm, system temperature=37°C, volume within BDC=365  $\mu$ L, volume in well plate used to submerge BDC=2,000  $\mu$ L, BDC membrane pore diameter=100 nm, BDC membrane pore density =  $8.913 \times 10^7$  pores/m<sup>2</sup>, BDC membrane thickness=125  $\mu$ m, BDC membrane area=490.873 mm<sup>2</sup>, concentration of 25 nm particles within BDC=3212 particles/mL, concentration of 50 nm particles within BDC=10939.5 particles/mL, concentration of 90 nm particles within BDC=281546.2 particles/mL, saline dynamic viscosity= $7.45 \times 10^{-5}$  kgf-s/m<sup>2</sup>. Initial starting conditions for the system under actively driven transport conditions were set to the same values as the passive transport condition, with the exception of the volume in the well plate=500  $\mu$ L that corresponds to only half of the BDC being submerged. Additionally, a 200  $\mu$ L volume of driving fluid was modeled on the exposed membrane of the BDC that was allowed to enter the BDC through the membrane resulting from gravitational forces. The ODE45 was solved over ~300 hours in 1 second timestep intervals.

#### *Analyses of IGV-001 BDC environment*

*m*IGV-001 cell proliferation was evaluated over time under adhered and non-adhered culture conditions. Briefly, 96-well plates were coated with an anti-adherence solution (Stemcell Technologies) or PBS prior to seeding with formulated *m*IGV-001 or untreated GL261 cells. Proliferation under both conditions was measured via metabolic activity determined using

the RealTime-GLO MT cell viability assay (Promega, WI). Nutrient availability within the BDCs were assessed by measuring residual glucose and protein content compared to standard GBM cell culture media or undiluted naïve mouse serum. Briefly, saline (control) BDCs were cultured *in vitro* as described in the methods section. After 3 h, the BDC contents were subject to glucose analysis using the Glucose-Glo Assay (Promega, WI) and to protein quantification using a Pierce Rapid Gold BCA Assay (ThermoFisher Scientific). Explanted saline (control) or *mIGV-001* BDCs were subject to the same analyses. Data is representative of 2-3 independent BDCs.

#### *sCalreticulin expression*

*m* and *hIGV-001* cells harvested from BDCs were washed twice in PBS + 5% FBS and then resuspended in buffer containing a PE-conjugated calreticulin mAB or concentration matched PE-conjugated isotype. Staining was allowed for 25 min at RT in the dark followed by the addition of 7-AAD for another 5 min. Stained cells were washed and then analyzed on a MACSQuant Analyzer 16 flow cytometer. Data analysis was performed using the Kaluza Analysis Software package. Analysis of surface calreticulin was performed only on 7-AAD-cells with *IGV-001* cells immediately after manufacturing were used as control to determine gating strategies.

*Therapeutic mIGV-001 in combination with anti-PD1 in the orthotopic GL261-luc2 mouse glioma model*

This study was designed by Invax, Inc., and executed by LabCorp in compliance with the National Institutes of Health and LabCorp's Animal Care. Female C57BL/6 albino mice from Envigo received an intracranial inoculation of  $1 \times 10^6$  GL261-luc2 cells to generate orthotopic tumors and 7 days later mice were randomized in to 4 groups to ensure that the mean tumor burden for all groups was within 10% of the overall mean tumor burden for the study population: (1) PBS-loaded BDC (i.e., Control) + control Ab; (2) mIGV-001 + control Ab; (3) PBS-loaded BDC (i.e., Control) + anti-PD1 Ab; (4) mIGV-001 + anti-PD1 Ab. mIGV-001 ( $1 \times 10^6$  GL261-luc2 cells/BDC, 1 BDC/mouse) or PBS-loaded BDCs were implanted in the flank on day 7 and left in place for 48 h. *InVivoPlus* rat IgG2a isotype control mAb (Clone 2A3) and *InVivoPlus* anti-mouse PD-1 mAb (Clone RMP1-14) were purchased from Bio X Cell and given i.p., 10 mg/kg, on days 7, 10, 14 and 17. Tumor burden was evaluated using weekly bio-luminescent imaging (BLI) of injected D-luciferin conversion with an IVIS Spectrum imager (Perkin Elmer, MO). Mice were euthanized individually before study termination when ethical abortion criteria were reached (e.g., body weight loss  $\geq 20\%$ , signs of sickness, distended cranium, severely impaired movement, severe respiratory distress or loss of righting reflex).

Aside from median survival time, Time to Progression (TP) was also used as a measurement of efficacy. TP data was analyzed by Kaplan Meier methods just as traditional lifespan data. The TP for an individual animal is the number of days between initiation of treatment and the day that the animal reached a selected evaluation size and may be ">" if mice survive to study termination if the evaluation size is not reached. The initiation of treatment is the day of first

treatment in the study. TP is a log-linear interpolation between the adjacent data points on either side of the selected tumor evaluation size. This normalizes the evaluation criteria for all animals. If an animal did not reach the selected evaluation size and was euthanized or found dead due to disease progression or lack of treatment tolerance, lifespan was utilized instead of TP. The median TP for a group is used to calculate the % Increase in Time to Progression (%ITP). A BLI flux of  $3.77 \times 10^8$  photons/s/cm<sup>2</sup>/sr was chosen to evaluate time to progression because this was close to the lethal signal for the majority of the study animals that showed disease progression in the evaluation.

#### *Orthotopic Hepa 1-6 hepatocellular carcinoma model*

This study was designed by Invax, Inc., and executed by Reaction Biology in Freiburg, Germany, in compliance by the Ethics Committee for Animal Experimentation, under the regional board Freiburg. Mice will be handled according to the German animal welfare law and the GV-SOLAS guidelines. Health monitoring of the animal facility will be done according to FELASA guidelines quarterly by examination of sentinel animals. Female C57Bl/6N (C57BL/6NCrl) mice from Charles River GmbH received either BDCs filled with PBS (control mice) or formulated *mIHC-001* ( $1 \times 10^6$  Hepa 1-6(Z1)-luc cells/BDC, 1 BDC/mouse). BDCs were subcutaneously implanted in the flank for 48 h followed by explantation and wound closing. On day 26 after BDC explantation, to generate orthotopic tumors, tumor cells ( $1.0 \times 10^6$  cells in 50  $\mu$ l PBS) were injected into the spleen of each mouse under anesthesia and allowed to migrate into the liver for 5 minutes via vena lienalis. Thereafter the spleen was resected to ensure that the tumor cells remain in the liver. During the study the growth of the orthotopically

Hepa 1-6(Z1)-luc tumors were monitored on every seventh day (+/- 1 day) starting on Day 10 using an IVIS® Lumina III bioluminescence imaging system (Perkin Elmer) with a CCD-camera. On day 102, 6 survivor animals (all from *mIHC*-001 group) as well as four naïve control animals were challenged with Hepa1-6(Z1) tumor cells ( $2.0 \times 10^6$  in 100  $\mu$ l PBS) implanted into the left mammary fat pad of each mouse. Tumor volumes were determined by caliper measurement according to the formula  $W^2 \times L/2$  (L = length and W = the perpendicular width of the tumor,  $L > W$ ).

### Figure Legends

**Supplemental Figure 1. Mice receiving preventative treatment with *mIHC*-001 experienced significantly longer survival and reduced tumor burden after orthotopic tumor challenge with Hepa 1-6(Z1)-luc cells.** Mice were exposed to either *mIHC*-001 (manufactured with  $1 \times 10^6$  Hepa 1-6(Z1)-luc cells/BDC) or PBS-loaded BDC (i.e., Control). BDCs were implanted in the flank and left in place for 48 h. Orthotopic tumor challenge was performed 26 days after BDC explantation. Intramammary tumor challenge with Hepa 1-6 (non-luciferase) was conducted on surviving mice of primary orthotopic challenge (n=6) on day 102. **(A)** Kaplan-Meier survival curves. Median OS for control mice=18 days vs. 67 for mice receiving *mIHC*-001. Log-Rank test  $**p < 0.01$ . **(B)** Individual mice bioluminescence signal showing reduced tumor burden in most mice receiving *mIHC*-001. **(C)** Tumor volume of intramammary-challenged animals. Days=days post-orthotopic tumor challenge. n=number of mice.

**Supplemental Figure 2. JAWSII murine DC co-cultured with *m*IGV-001 present upregulated expression of DC maturation markers.** LPS pretreated (100 ng/mL) JAWSII cells were exposed to additional 10 µg/mL of LPS (i.e., JAWSII), *m*IGV-001 placed directly on cells (i.e., JAWSII + *m*IGV-001), or PFA-fixed *m*IGV-001 placed directly on cells (i.e., JAWSII + Fixed *m*IGV-001) for 24 h and maturation marker expressions were evaluated by flow cytometry. **(A)** CD80, **(B)** CD86, and **(C)** MHC-II. **(D)** Representative flow cytometric raw data (red histogram=isotype control; green histogram=antibody stain). Results are presented as the mean fold change of 3 independent experimental setups each with 3 replicates per condition normalized to its respective JAWSII alone condition +/- SD. Statistical analysis was performed using One-way ANOVA with multiple comparisons (using Pre-treated condition for comparison), \* $p < 0.05$ , \*\* $p < 0.01$ .

**Supplemental Fig. 3. Cellular debris and particle diffusion in IGV-001.** Particle concentration in the supernatant of *h*IGV-001 (T98G) BDC content after *in vitro* culture for 48h was analyzed on a Malver NanoSight NS300 nanoparticle tracking analysis (NTA) instrument. Nanoparticle transport was modeled using the Kedem-Katchalsky system of equations for solute transport kinetics across semi-permeable membranes in MATLAB 2022a (Mathworks™). **(A)** Distribution of tumor particle sizes in *h*IGV-001(T98G) BDCs supernatant from T98G GBM cells. **(B)** Theoretical concentration of 25, 50 & 90 nm particle-sizes diffusion under passive conditions. **(C)** Theoretical concentrations of 25, 50, & 90 nm particle-size diffusion under dynamic conditions.



**Supplemental Fig. 4. Physical stressors contribute to cell death in *mIGV-001*.** Manufactured *mIGV-001* cells were cultured in adherent and non-adherent wells and cell proliferation was analyzed via metabolic activity using the RealTime-GLO MT cell viability assay. Supernatants from *mIGV-001* explanted from mice were analyzed for glucose (Glucose-Glo assay) and protein content (BCA assay) as surrogates for overall nutrient availability. **(A)** Proliferation of *mIGV-001* cells under non-adherent conditions and conventional cell-treated wells. **(B)** Glucose concentration inside implanted BDCs compared to standard culture media. **(C)** Protein concentration inside implanted BDCs compared to mouse sera. Analysis of nutrient availability inside *in vitro* cultured BDCs for **(D)** glucose and **(E)** protein content after equilibration (~3 h) with surrounding medium. Results are presented as mean +/- SD of 1 experiment with 3 biological replicates or 2 explanted BDCs. Statistical analysis was performed using either standard unpaired or Welch's corrected t-test, \* $p < 0.05$ , \*\*  $p < 0.01$ , \*\*\* $p < 0.001$ , \*\*\*\* $p < 0.0001$ .

**Supplemental Fig. 5. Surface calreticulin (sCRT) expression in *m* or *hIGV-001*.** sCRT expression levels over time, in *m* or *hIGV-001* GBM 7-AAD- cells were analyzed by flow cytometry. Data representative of 1 out of 3 biological replicates.

